Predicting Microstructure-Creep Resistance Correlation in High Temperature Alloy over Multiple Time Scales

Prof. Vikas Tomar (PI) & Hongsuk Lee &Sudipta Biswas

School of Aeronautics and Astronautics, Purdue University

Prof. Jian Luo (co-PI) & Naixie Zhou

University of California, San Diego & Clemson University

Program Manager: Dr. Jason Hissam
Grant No. : DEFE0011291

Long Term Creep in Microstructures

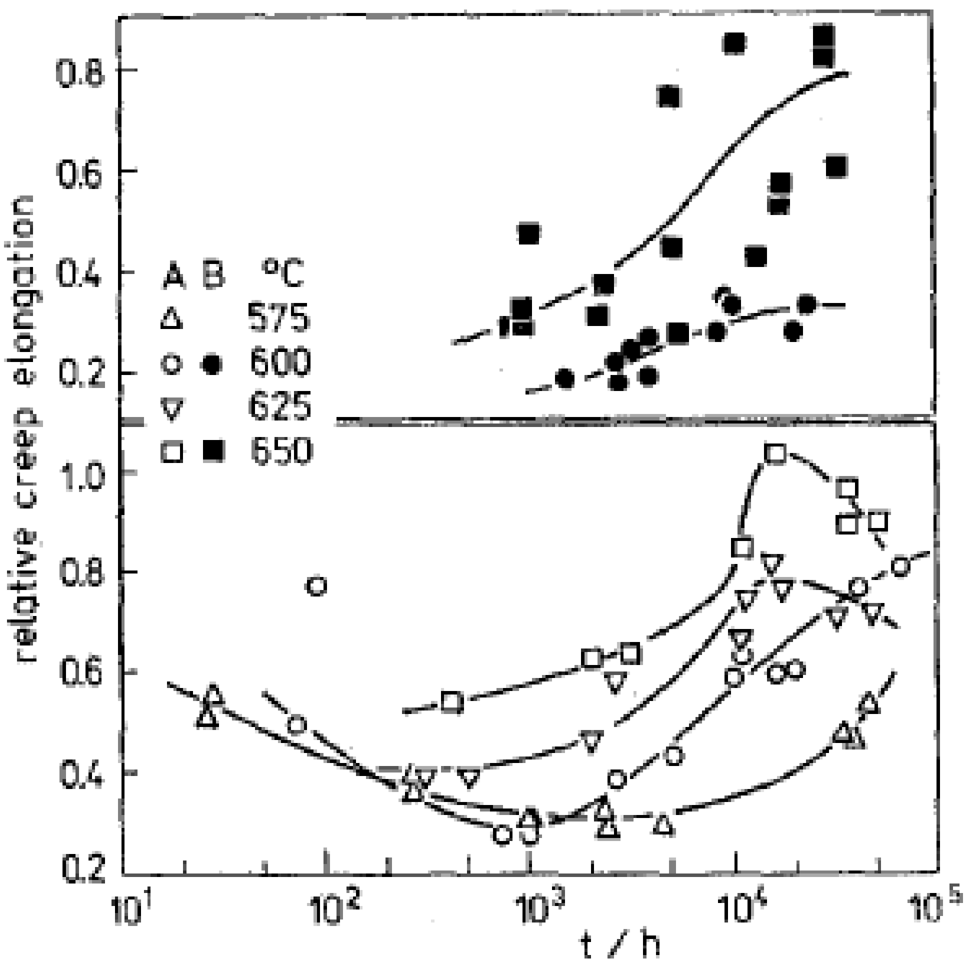

Sobotka, 1985, AISI 316 LN Steel

A detailed analysis of microstructure and fractures showed that the developing intergranular precipitation and the following coarsening of grain boundary particles of $M_{23}C_6$, Cr_2N and especially of the sigma phase are responsible for the significant changes of both creep and impact fractures from the point of view of their plasticity.

Long Term Creep in Microstructures

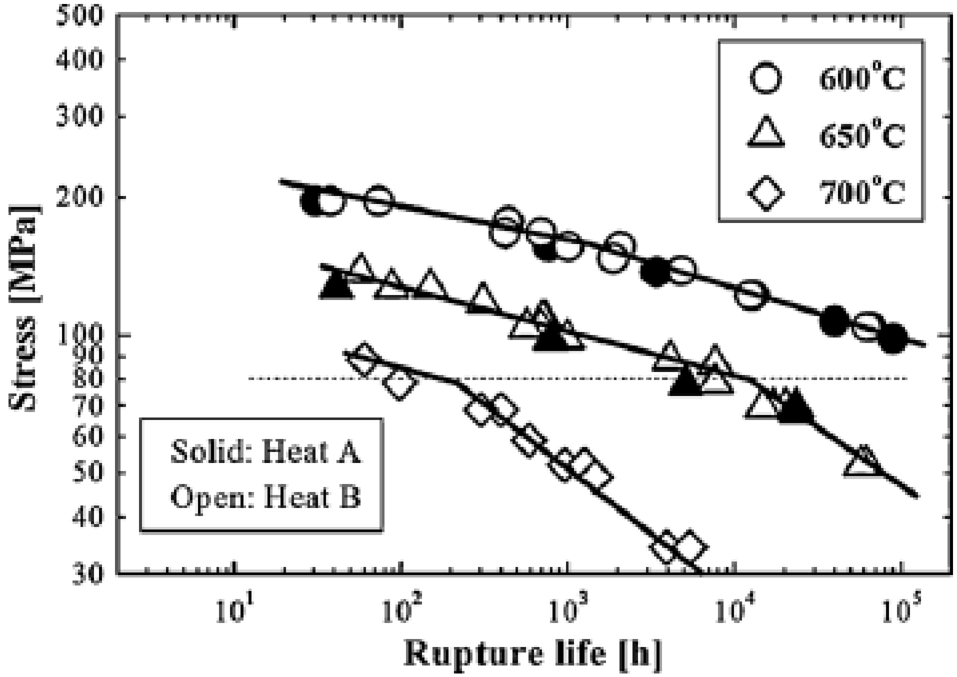

Fig. 1. Stress and temperature dependence of creep rupture life in Gr.91 steel.

Igarashi, 2011

The cause of the breakdown of creep strength has been studied in Gr.91 steel. The results show that the contribution of the static recovery of subgrains to creep deformation causes the breakdown of creep strength. The subgrain boundaries are mainly stabilized by $M_{23}C_6$ and MX precipitates. MX precipitates are thermally stable even in the time range when coarsening of subgrains takes place. Whereas $M_{23}C_6$ precipitates are not thermally stable and the aggregation of $M_{23}C_6$ precipitates takes place in the time range when coarsening of subgrains happens. Therefore, loss of pinning force from $M_{23}C_6$ precipitates is responsible for the static recovery of subgrains. MX has nothing to do with the static recovery. The

Proposal Research Workflow

Task-3

Theoretical Framework to Characterize GB Segregation

Task-1

Nanocrystalline Ni and Bulk W Based Alloy Control Sample Preparation

Task-4

Microstructure Level Multiscale Modeling to Predict Effect of GBs on Embrittlement, Creep, and rupture

Task-2

In-Situ Microstructural Testing of GB Evolution and Strength

U.S. DEPARTMENT OF ENERGY

Task 1:
Fabrication and Characterization of Control Samples

UC San Diego

- Task 1, Part A: Nanocrystalline Ni and Ni-W Foils (Synthesized by Electrodeposition)
- Task 1, Part B: Bulk W based Alloys (Synthesized by Ball Milling + SPS)

1 Task 1: Fabrication and Characterization of Control Samples – Part A

Preparing Nanocrystalline Ni and Ni-W Specimens for Mechanical Test

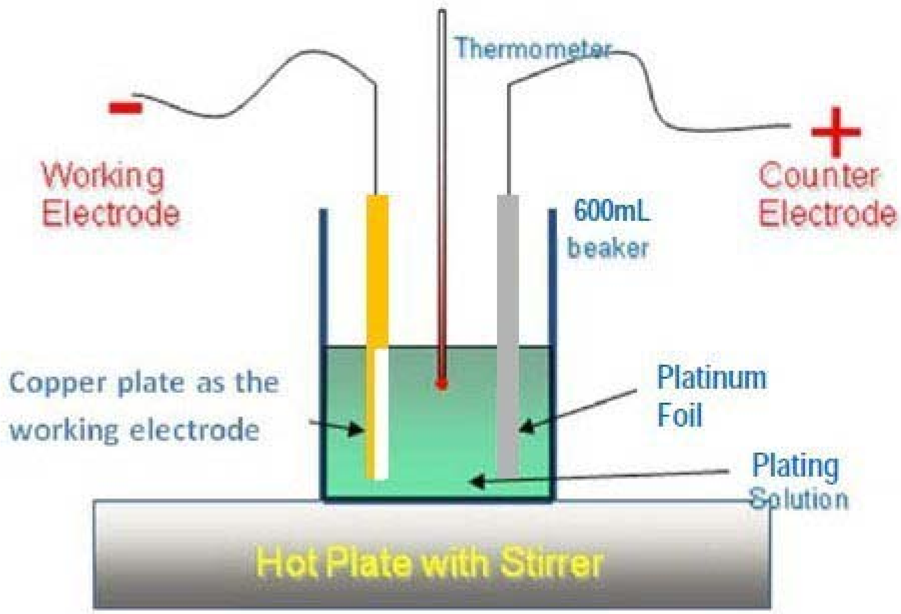

Temperature: 65 °C

Deposition time:
30 min to 2h

Chemicals	Weight(g/L)
$NiSO_4.6H_2O$	300
$NiCl_2.6H_2O$	45
H_3BO_3	45
Saccharine	5
Sodium Lauryl Sulfonate ($CH_3(CH_2)_{11}OSO_2Na$)	0.25

Current		Time (ms)	Peak (A/cm^2)
Forwards	On	5	0.4
	off	15	

El-Sherik, *et* al., J of Materials Science 30, 5743 (1995)

Slide 6

1 Jian Luo, 4/17/2015

Free-Standing Nanocrystalline Ni Specimens

Sent to Purdue for Creep Testing…

Grain Size (from the Scherrer equation) is ~18 nm.

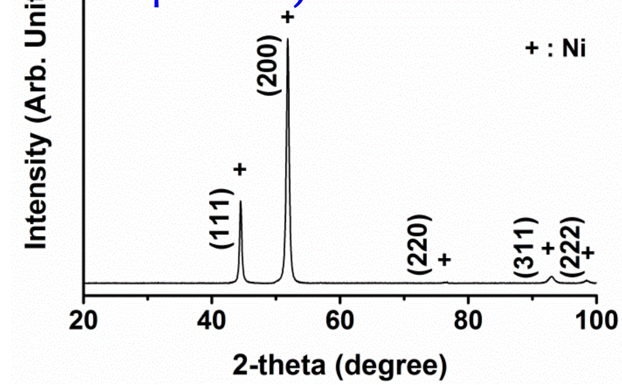

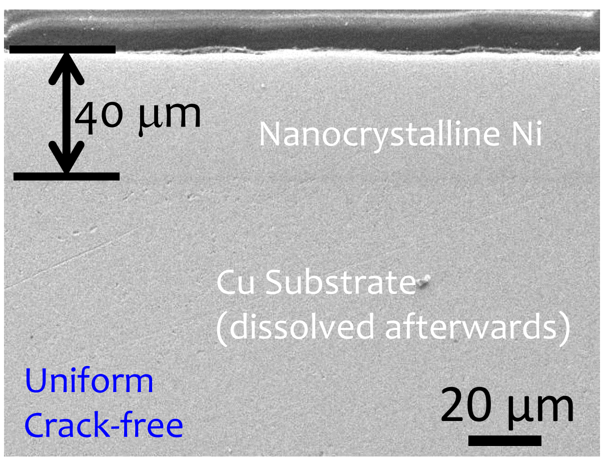

30min

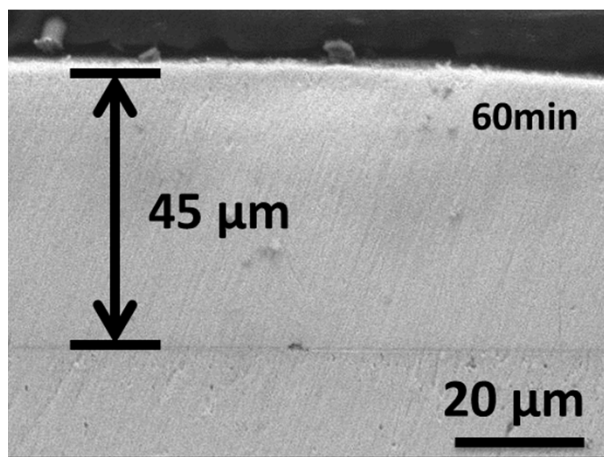

60min

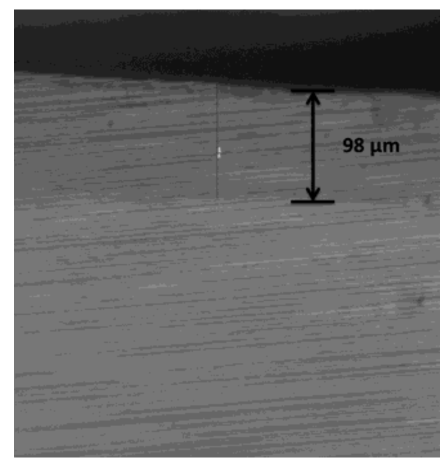

120min

Two-step to Prepare Bulk Nanocrystalline W Alloys

Nanocrystalline Powders

Bulk Nanocrystalline Material

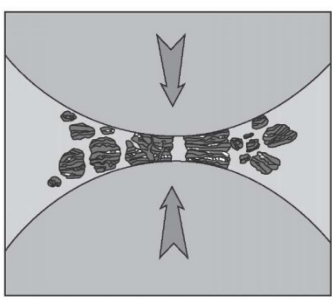

High Energy Ball Milling

Pressureless Sintering

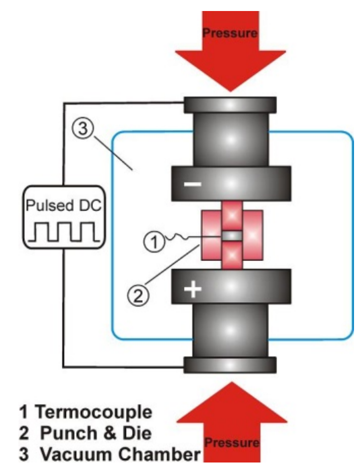

Spark Plasma Sintering

Task 1: Fabrication and Characterization of Control Samples – Part B

Bulk Nanocrystalline W Alloys

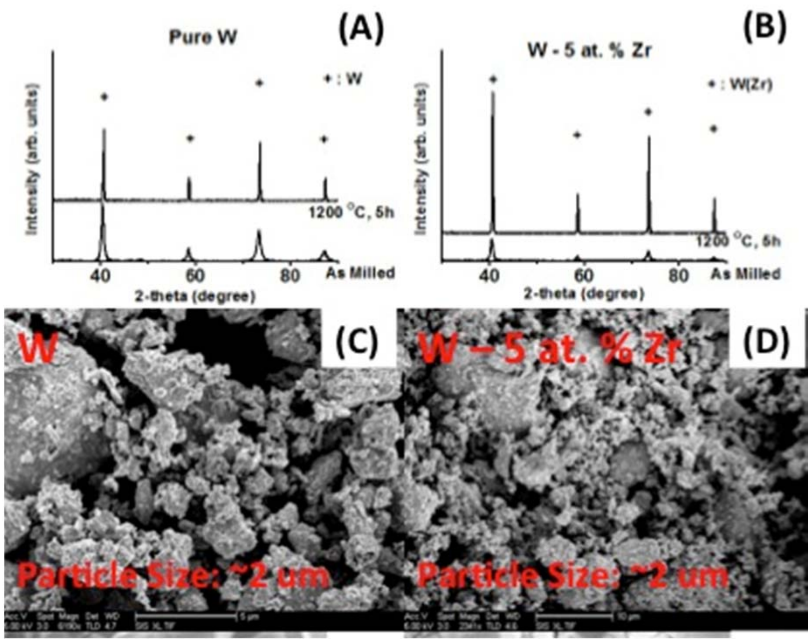

Ball Milled Powder

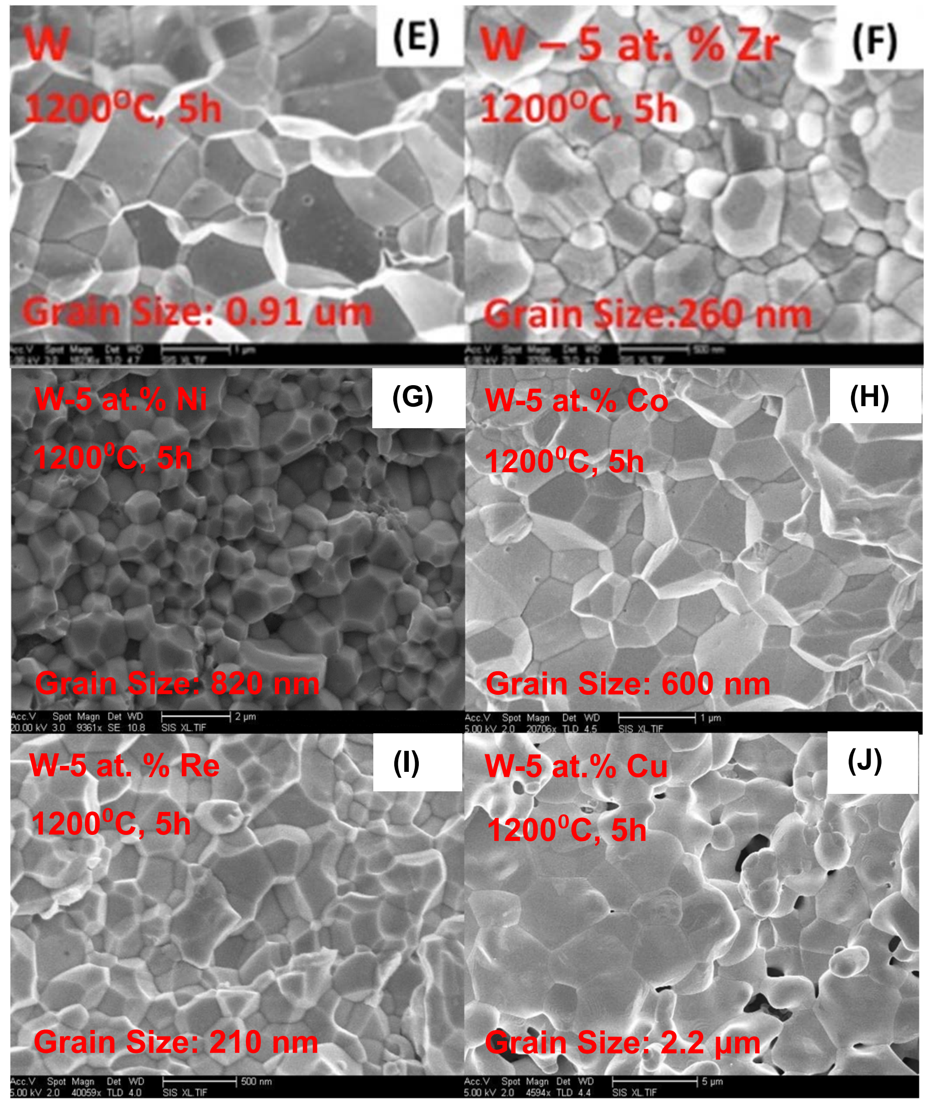

Pressureless Sintered Samples

Task 1: Fabrication and Characterization of Control Samples – Part B

Bulk Nanocrystalline W Alloys

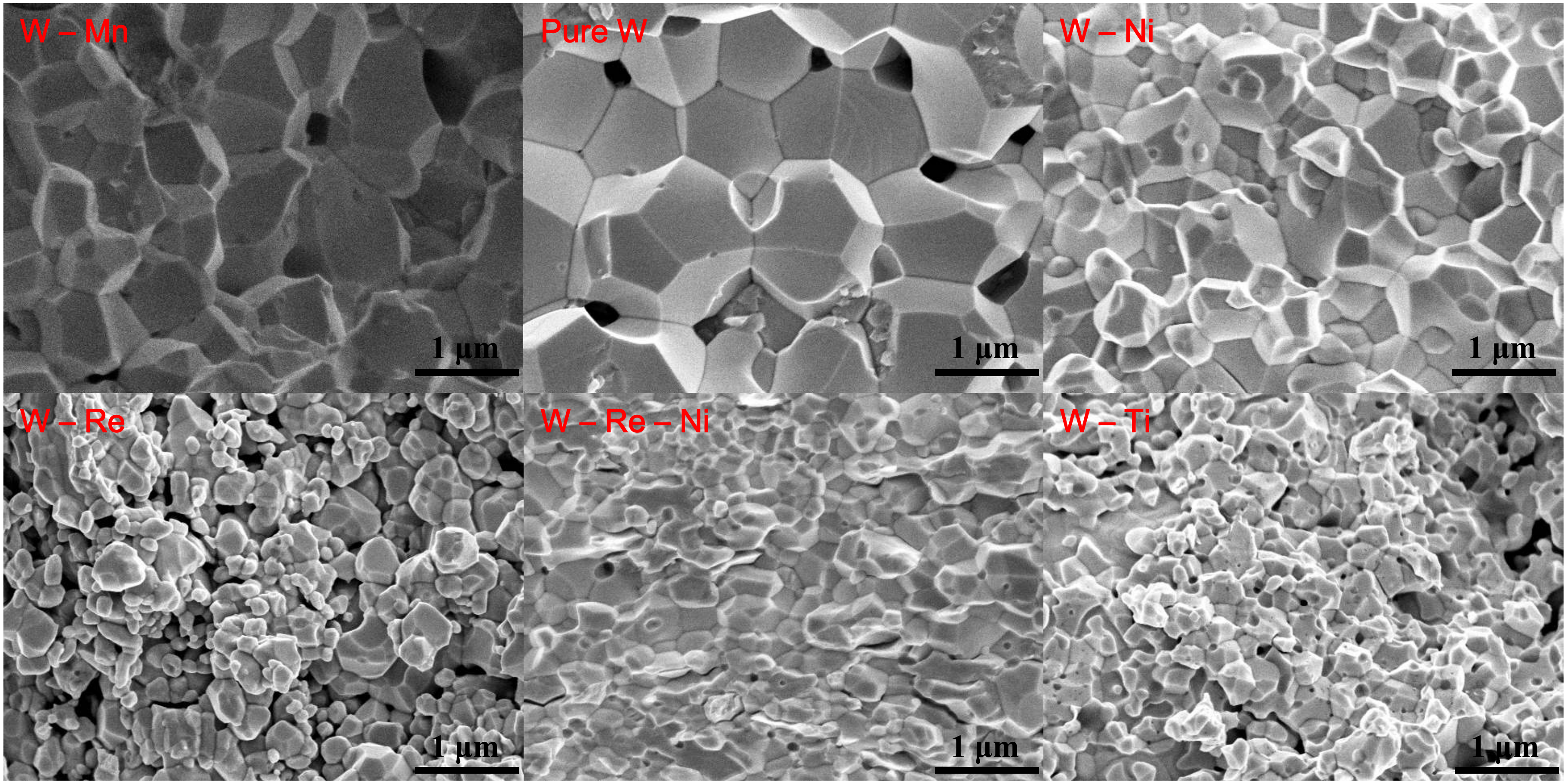

Spark Plasma Sintered Samples

Task 1, Part B Extension – Testing of Bulk Nanocrystalline Specimen (Currently in Progress @ UCSD)

Creep Test Setup

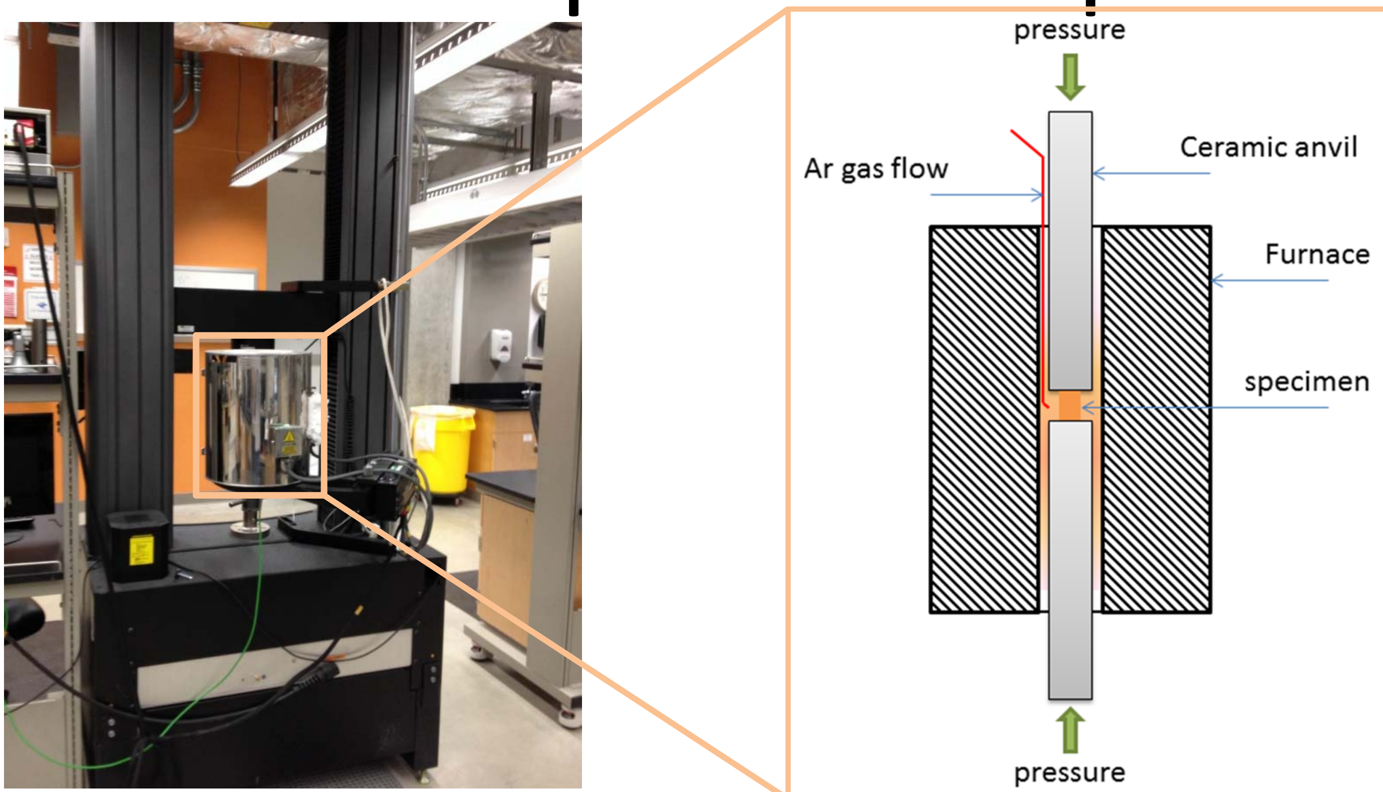

INSTRON Instrument Equipped with Heating Furnace

Planned Experiments:

- The creep tests for the specimens pure W, W-5%Ni, W-5%Ti, W-5%Co, W-5%Re and W-5%Cu will be performed at elevated temperature 400° C and/or 750° C.
- Creep data will be collected to evaluate the mechanical properties of the W alloys with different doping elements.
- Moreover, the microstructure evolution of creep tested W alloys specimens will be characterized by SEM and TEM.

Task 2-High Temperature Nanoindentation Tests

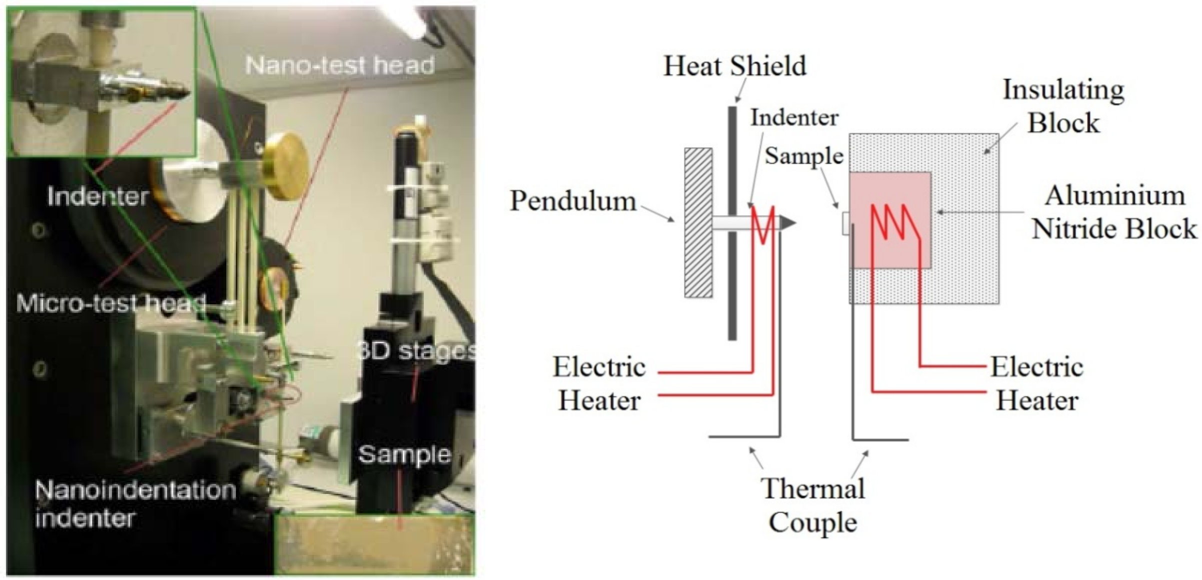

(a.)

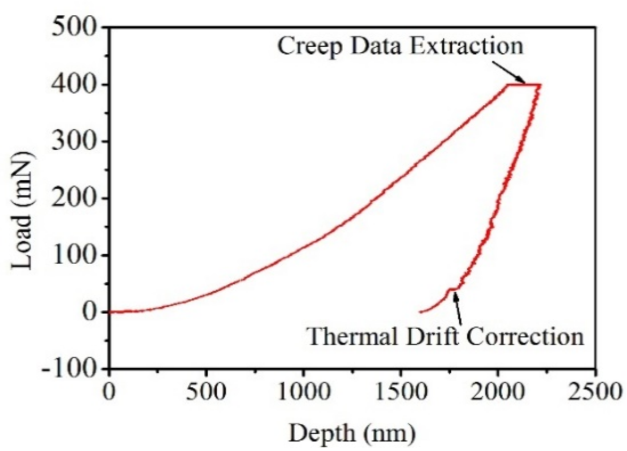

(b.)

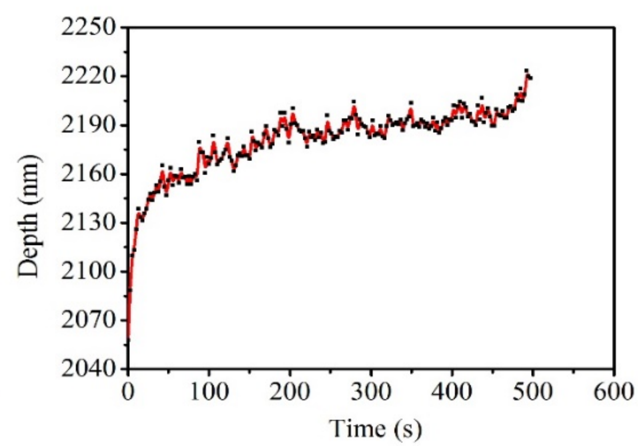

(c.)

Task 3:
A New Theoretical Framework to Characterize GB Segregation

UC San Diego

- Task 3, Part A: The Classical GB Segregation Model (Assessments of W alloys with the Wynbaltt-Chatain Model)
- Task 3, Part B: Non-Classical High-*T* GB Segregation (Coupled with GB Premelting/Interfacial Disordering

Task 3, Part A: Classical GB Segregation Model
Assessment of W based Alloys by the Wynblatt-Chatain Model

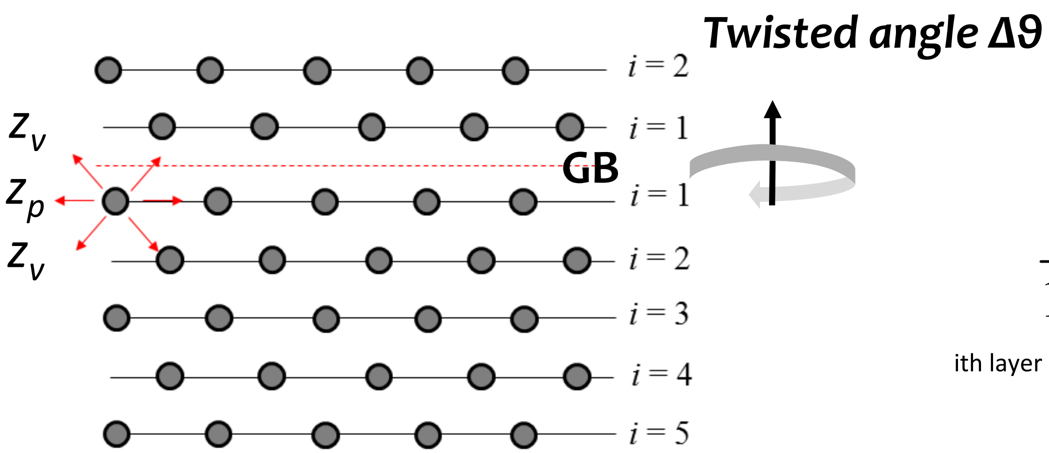

A Mclean type segregation equation

$$\frac{X_i}{1-\underline{X_i}} = \frac{X_\infty}{1-\underline{X_\infty}} \exp\left(-\frac{\Delta H_i^{seg}}{kT}\right)$$

ith layer composition — Bulk composition

GB absorption $\quad \Gamma_{GB} = 2\sum_i \left(X_i - X_\infty\right)$

Segregation Enthalpy

bonding energy difference — **strain energy** — **Solute-dopant interactions**

$$\Delta H_i^{seg} = \begin{cases} -0.5Q(e_{BB}-e_{AA})z_v - \Delta E_{el}^1 + 2\omega_S \begin{bmatrix} zX_\infty - z_p X_1 - z_v X_2 \\ -(1-Q)z_v X_1 - \frac{1}{2} Q z_v \end{bmatrix} & i = 1 \\ -\Delta E_{el}^i + 2\omega_S (zX_\infty - z_p X_i - z_v X_{i+1} - z_v X_{i-1}) & i > 1 \end{cases}$$

W-Co (Co-doped W) Alloy

Phase diagram

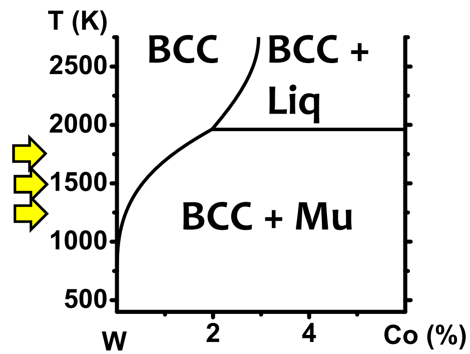

GB energy

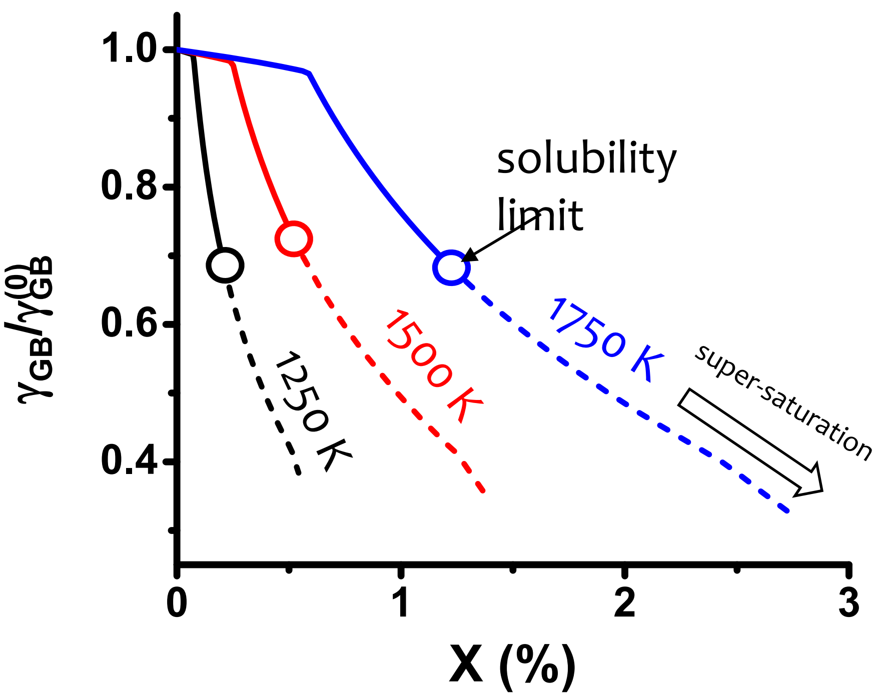

GB absorption

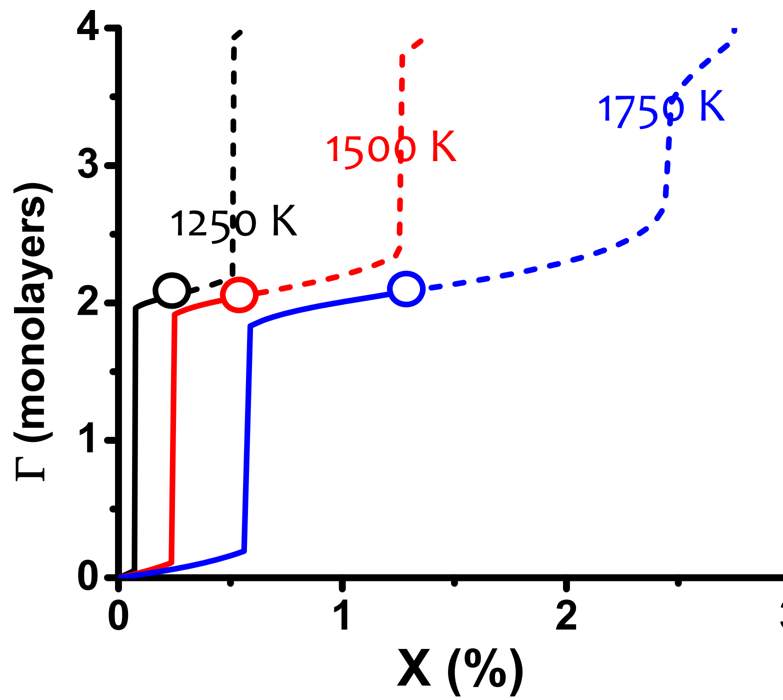

W-Cr Alloy

Phase diagram

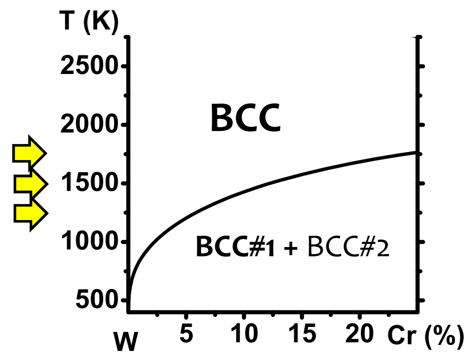

GB energy

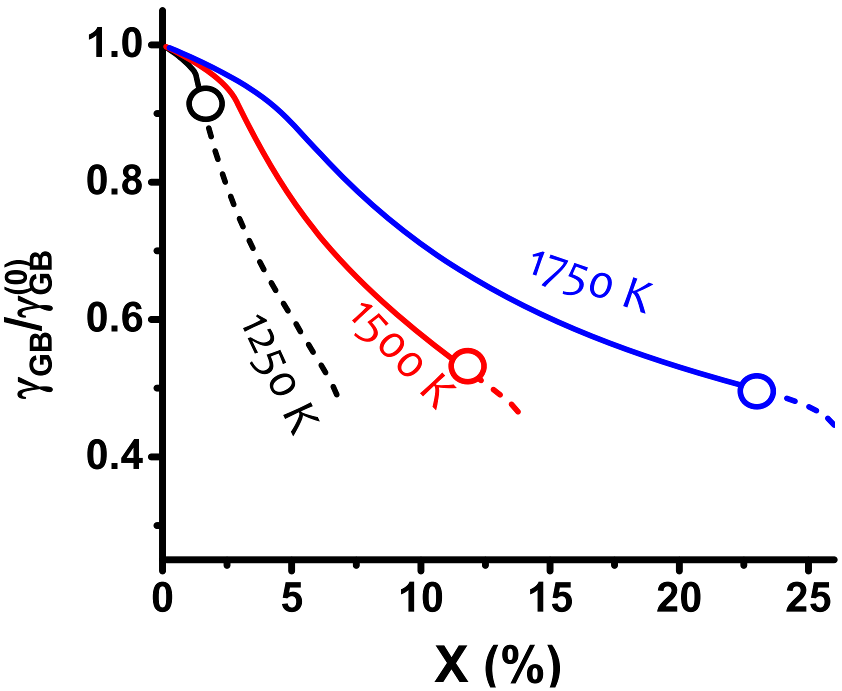

GB absorption

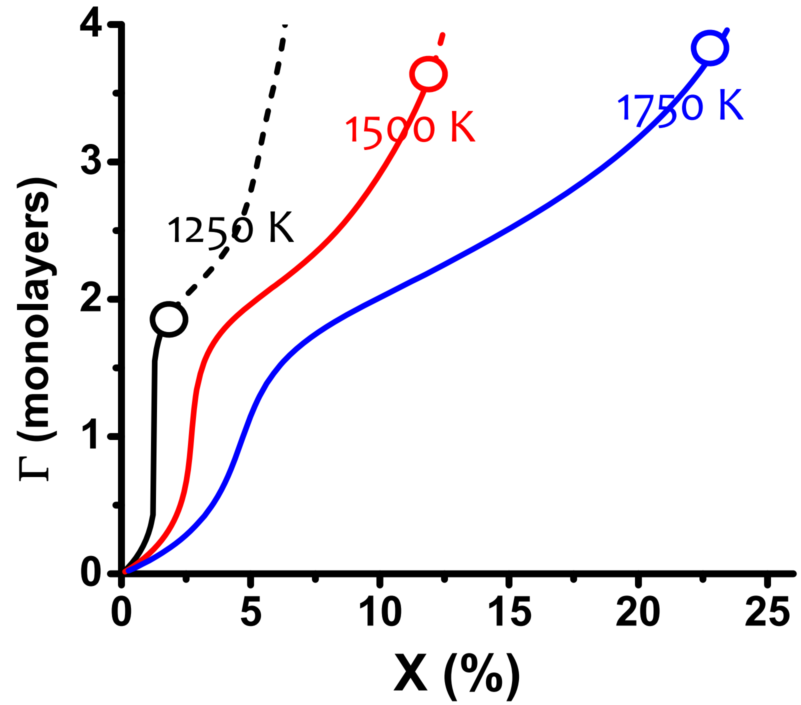

W-Fe Alloy

Phase diagram

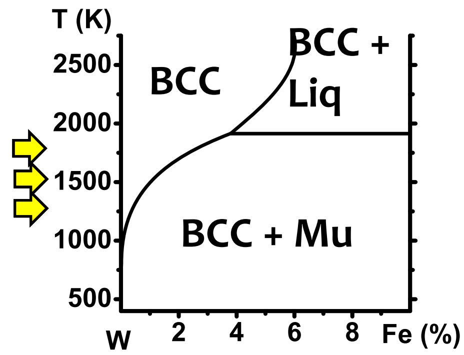

GB energy

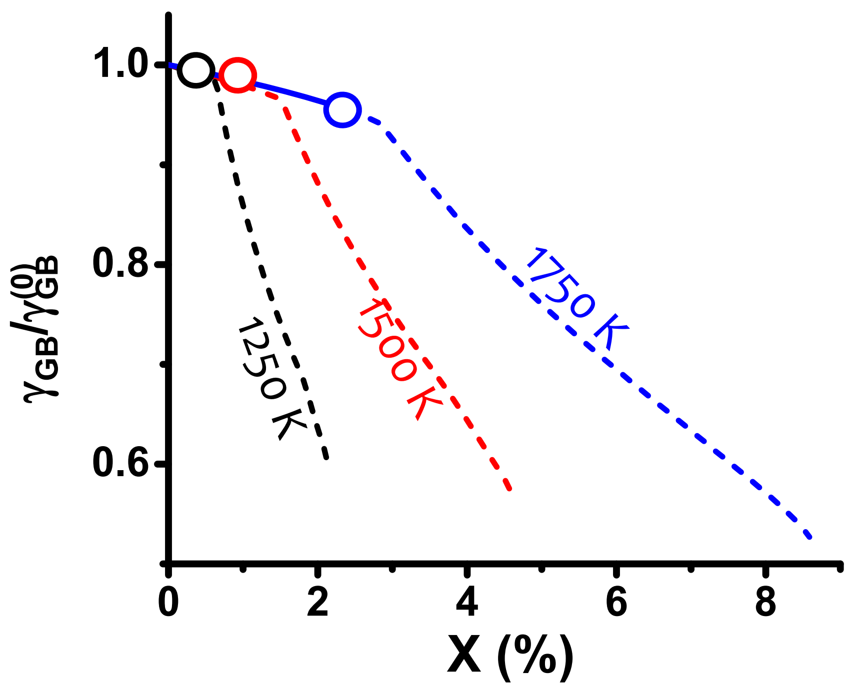

GB absorption

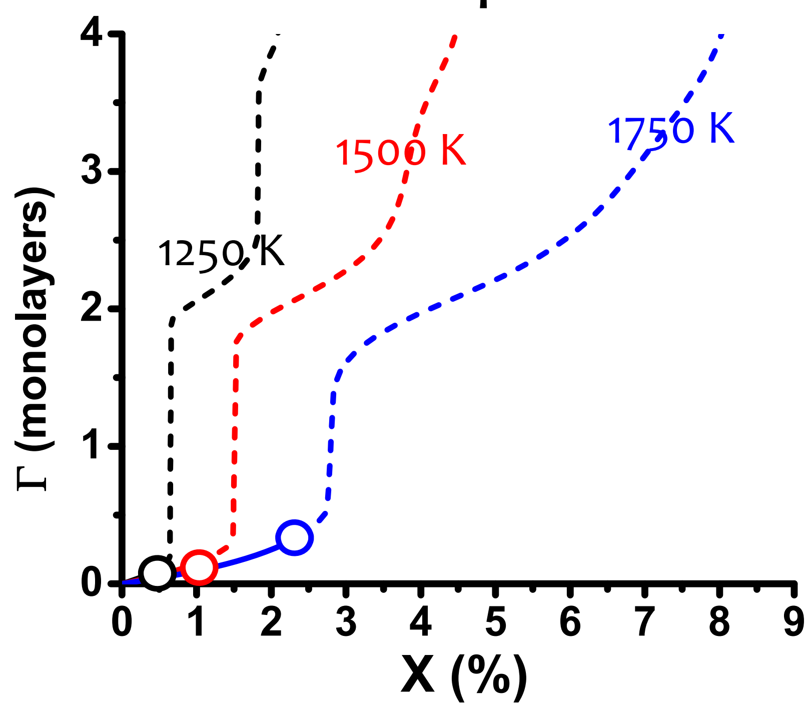

W-Zr Alloy

Phase diagram

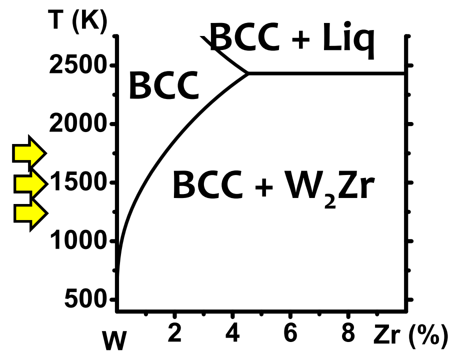

GB energy

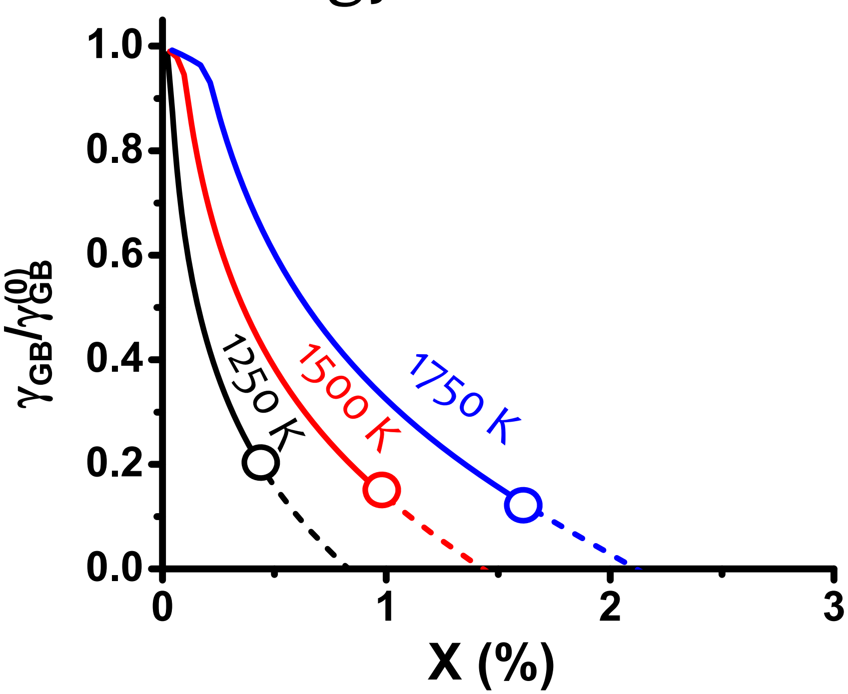

GB absorption

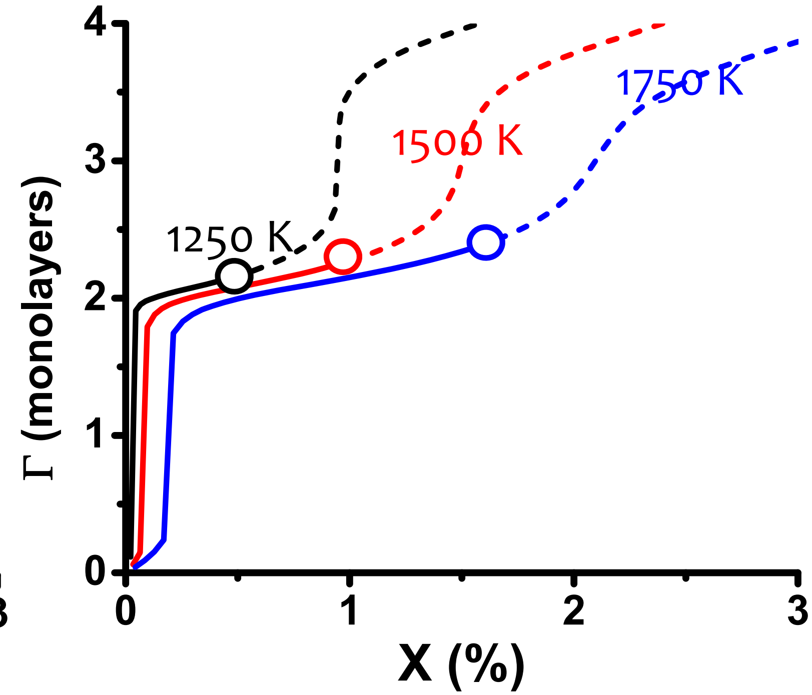

Task 3, Part B: High-T Segregation + GB Disordering

Develop a thermodynamic framework to predict
a "new" type of high-*T* (premelting-like) GB segregation
Luo *et al.* at Clemson/UCSD

Multiscale modeling to characterize microstructure-dependent creep
Tomar *et al.* at Purdue

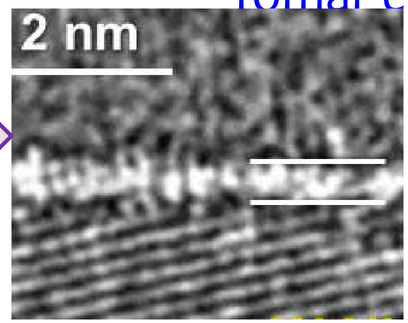

Discovered by the Luo group
Appl. Phys. Lett. 2005
Acta Mater. 2007

Thermodynamic Principle

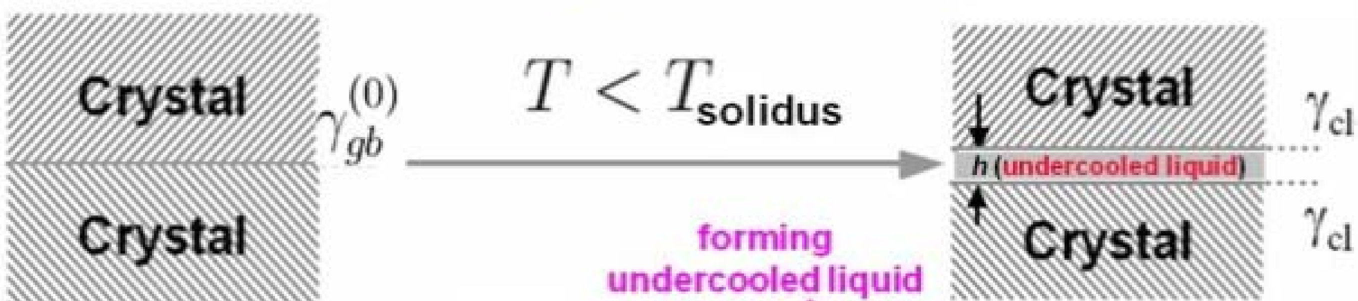

A subsolidus quasi-liquid film is **thermodynamically stable** if:

$$\Delta G_{\mathrm{vol.}} \cdot h < -\Delta\gamma \equiv \gamma_{gb}^{(0)} - 2\gamma_{cl}$$

Prior Relevant Studies

Thermodynamic Model for High-*T* GB Disordering

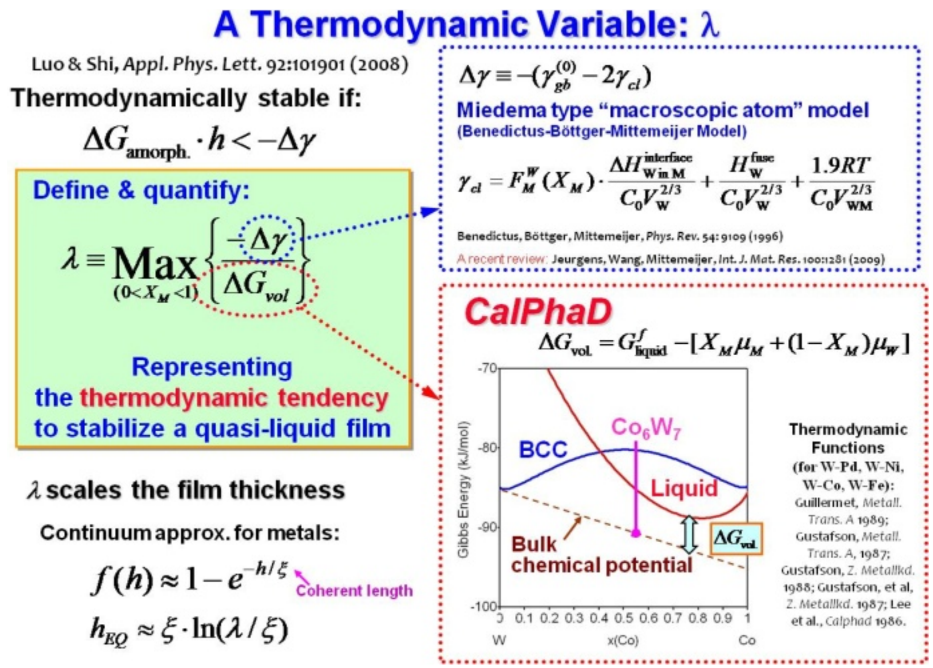

See: related review article
"Developing Interfacial Phase Diagrams for Applications in Activated Sintering and Beyond: Current Status and Future Directions"
Journal of the American Ceramic Society
95: 2358 (2012)

Computed GB λ Diagrams to Represent Levels of GB Disorder

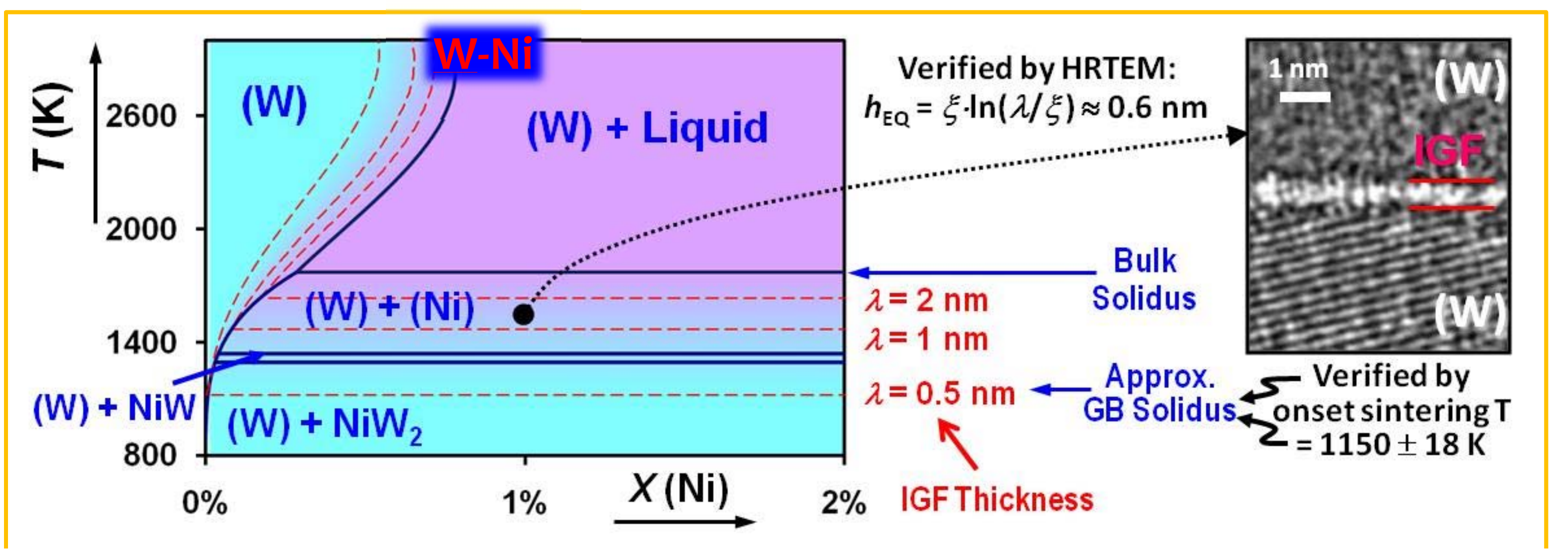

The Model for Ternary Alloys

Interfacial energies

Miedema type model modified to use CALPHAD parameters

$$\Delta\gamma = 2\gamma_{\mathrm{cl}} - \gamma_{GB}^{(0)}$$

$$\gamma_{GB}^{(0)} \approx \sum_i X_i^C \gamma_{GB,i}^{(0)} + \overbrace{\frac{Q}{C_0 V^{2/3}} \sum_{i\neq j} X_i^C X_j^C \Omega_{i-j}^C}^{\text{excessive interaction energy}}$$

$$\gamma_{cl} \approx \gamma_{cl}^{(0)} = \frac{1}{C_0 V^{2/3}} \left[\sum_i X_i^C \underbrace{\left(\Delta H_i^{fuse} + \sum_{i\neq j} X_j^L \Omega_{i-j}^L \right)}_{i\text{-}j\text{ interfacial energy}} - \frac{1}{2} \underbrace{\left(\sum_{i\neq j} X_i^L X_j^L \Omega_{i-j}^L + \sum_{i\neq j} X_i^C X_j^C \Omega_{i-j}^C \right)}_{\text{reference energy}} \underbrace{+1.9RT}_{\text{entropy due to near interface ordering}} \right]$$

Bulk free energy of undercooled liquid

$$\Delta G_{\mathrm{amorph}}^{(\mathrm{mol})} = G^{\mathrm{L}}(\mathbf{X}_{film}^{L}) - \sum_i \mu_i^C X_i^{\mathrm{L}}$$

Multicomponent free energy function built based on binary CALPHAD database

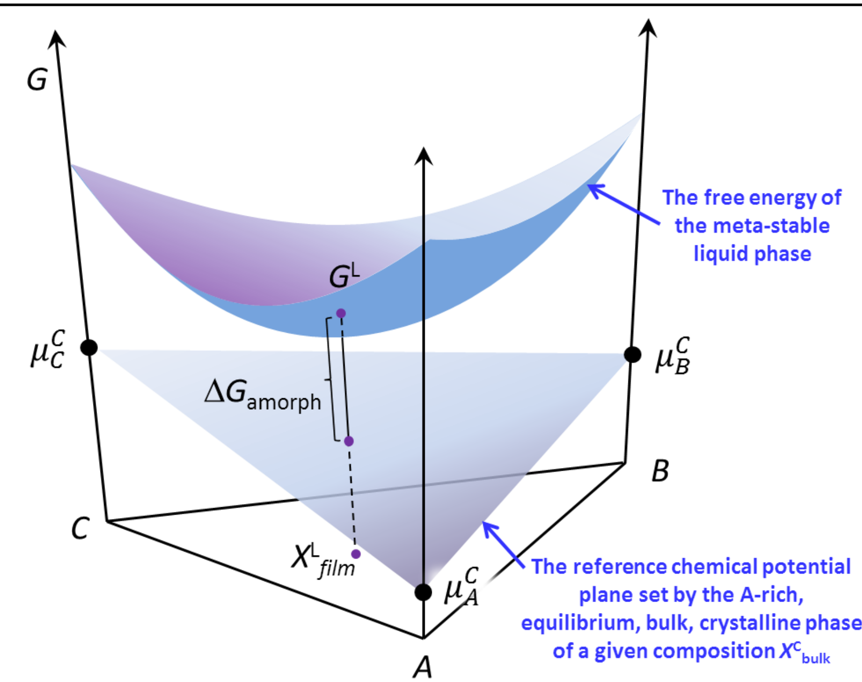

The Effects of Co-Doping on Enhancing or Suppressing GB Disorder

The effects of adding a co-alloying element X to W-Ni

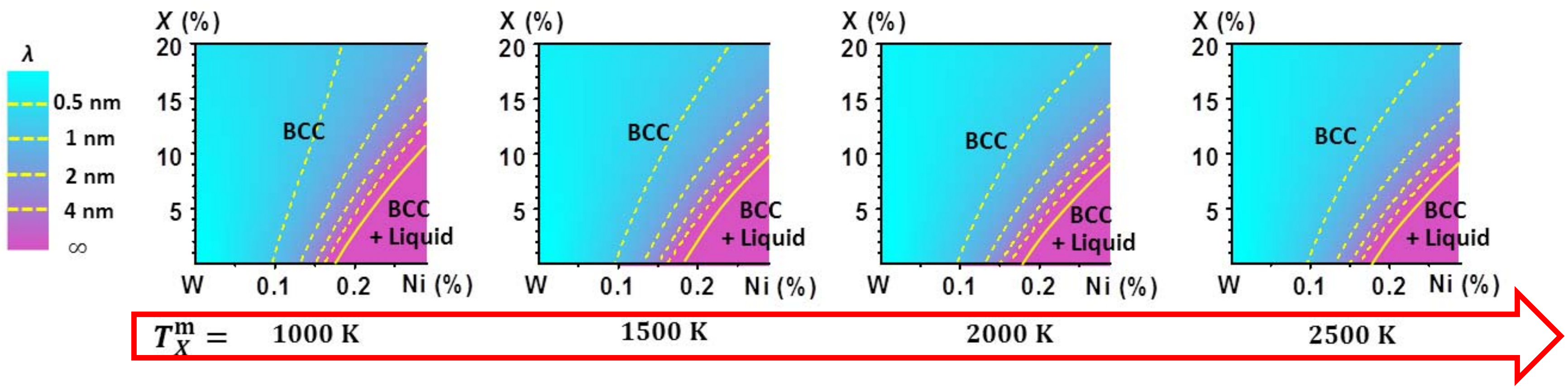

Change the melting point of the co-alloying element *X*

Assumptions:

X mix ideally with W and Ni

X mix ideally with Ni and (- $\Omega^{\mathrm{BCC}}_{\mathrm{W}\text{-}X}$) = $\Omega^{\mathrm{L}}_{\mathrm{W}\text{-}X}$ 50 kJ/mol

Zhou & Luo,
Acta Materialia 2015

The Effects of Co-Doping on Enhancing or Suppressing GB Disorder

The effects of adding a co-alloying element *X* to W-Ni

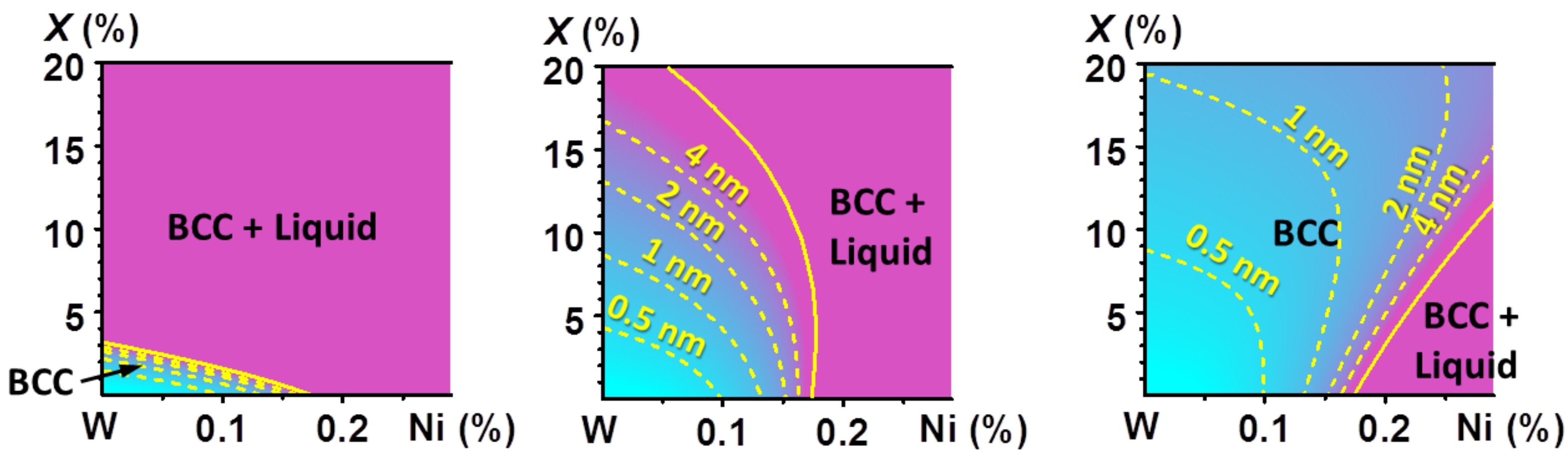

Ω^{L}_{X-W} = 0 KJ/mol -25 KJ/mol -50 KJ/mol

Ω^{BCC}_{X-W} = +50 KJ/mol +25 KJ/mol 0 KJ/mol

Change W-X interaction parameters

Zhou & Luo,
Acta Materialia 2015

Task 4: Multiscale Models for Rupture Strength and Long Term Creep

Models of Rupture
Based on GB Strength

Quantum Mechanics
Based on
Thermodynamics

Predictions Validated
with in-situ and ex-
situ experiments

Models of Creep Evolution While
Incorporating Interface Physics
and Mechanics

➢Quantum mechanical calculation of GB Strength

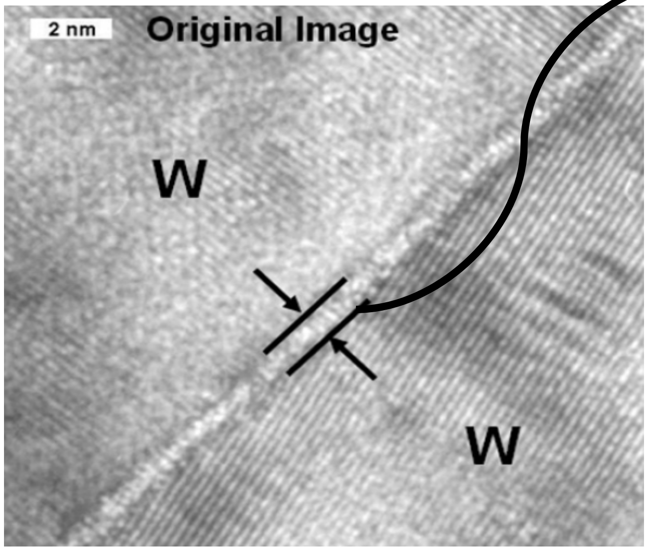

[Vivek K. Gupta and et al., 2007]

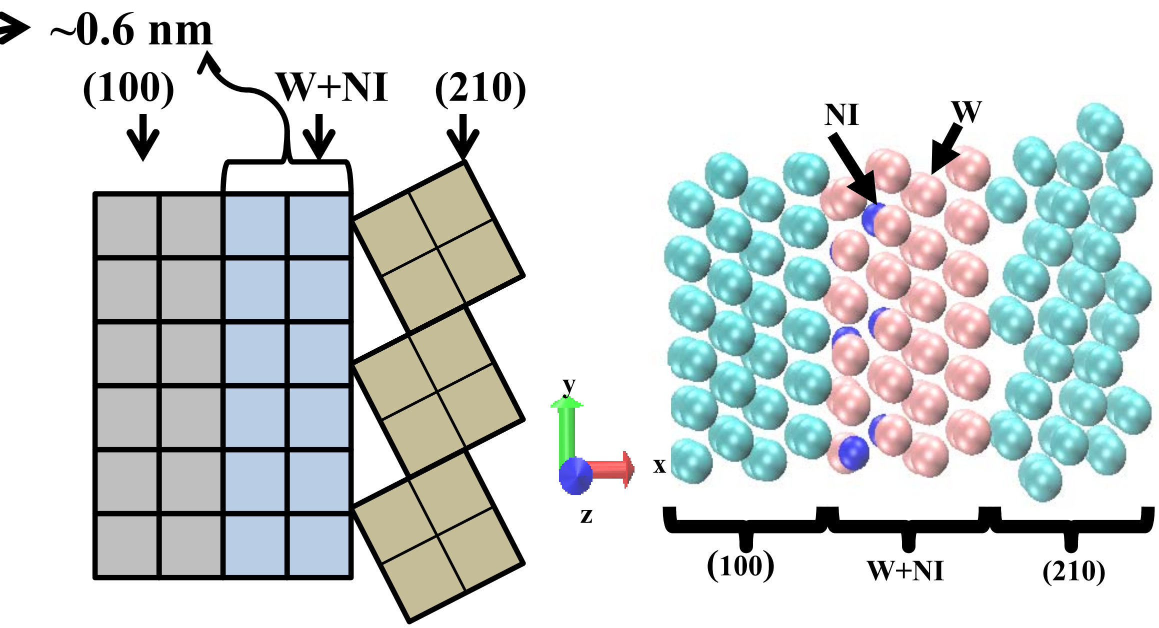

- ❖ time step: 5 a.u. , total 2000 steps — Becquart and et al., 2006
- ❖ cutoff energy for wavefunction : 350 eV — Nose and Shuichi, 1984
- ❖ Nose-Hoover thermostat : 300K, 400K, 500K, 600K — Hoover and William, 1985
- ❖ electronic fake mass for CPMD : 400 a.u. — Perdew and et al., 1996 — Vanderbilt and David, 1990
- ❖ number of k-points for integration over Brillouin zone : 32x32x32 — Monkhorst and Pack., 1996

➢Stress – strain relation

(1) Unsaturated Ni - W

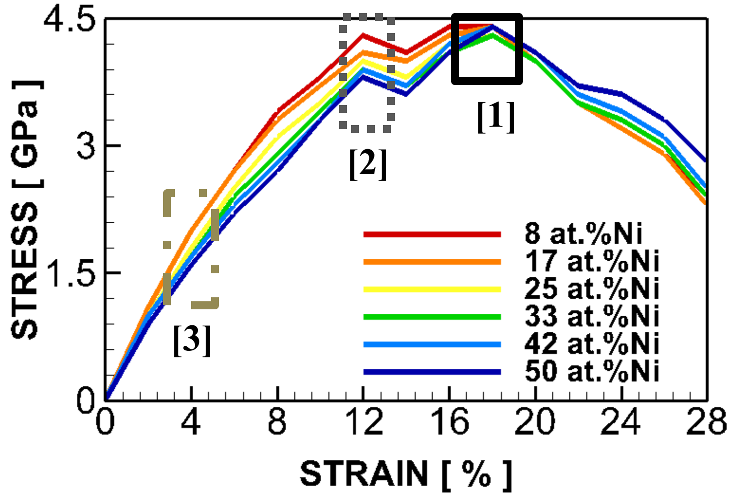

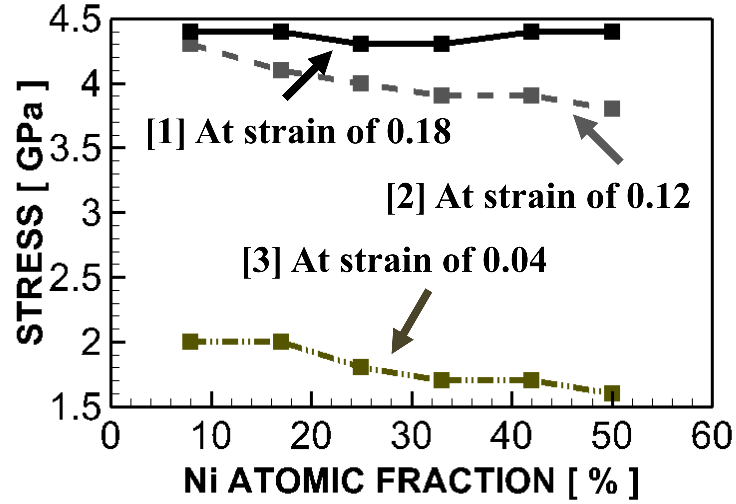

Yield strength: at strain 4%,
First peak: at strain 12%
Yield strength and first peak’s values have dependent on the Ni volume fraction.
Second peak: at strain 18%
The second peak’s values are not depend on the Ni volume fraction.
Ultimate tensile strength : strain of 12~18%
The maximum tensile strength is not affected by Ni volume fraction for the unsaturated W-Ni.

(2) Saturated Ni - W

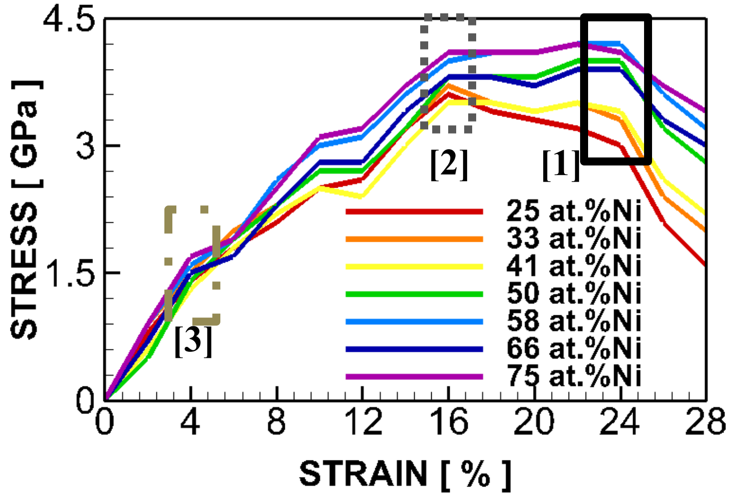

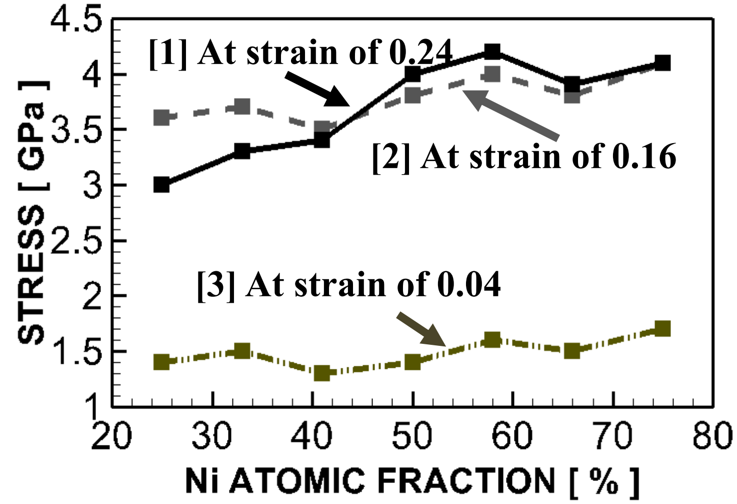

Yield strength: at strain 4%,
First peak: at strain 16%
Yield strength and first peak's values have dependent on the Ni volume fraction.
Second peak: at strain 24%
The second peak's values have the largest dependence on the Ni volume fraction.
Ultimate tensile strength : strain of 16~24%
The maximum tensile strength is not affected by Ni volume fraction for the saturated W-Ni.

➢Electron density distribution

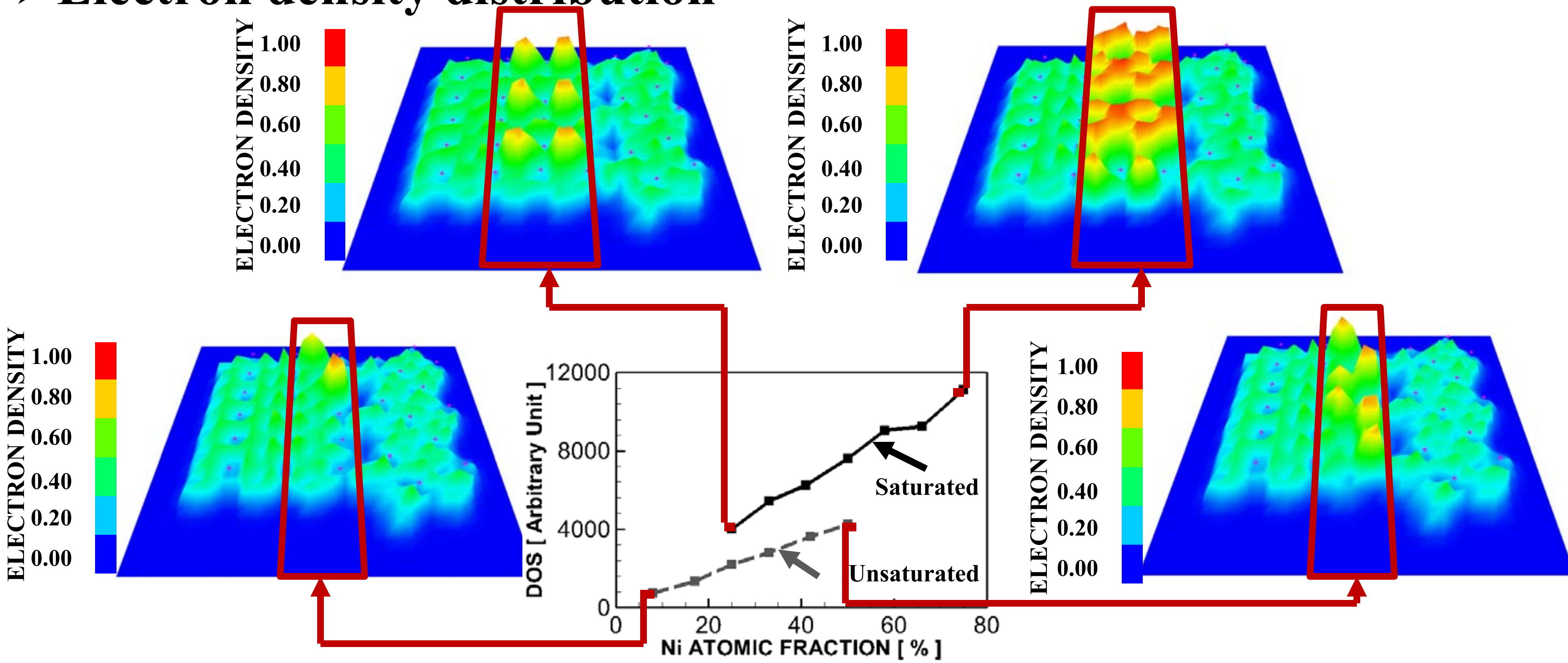

➢Electron density of states (f-orbital)

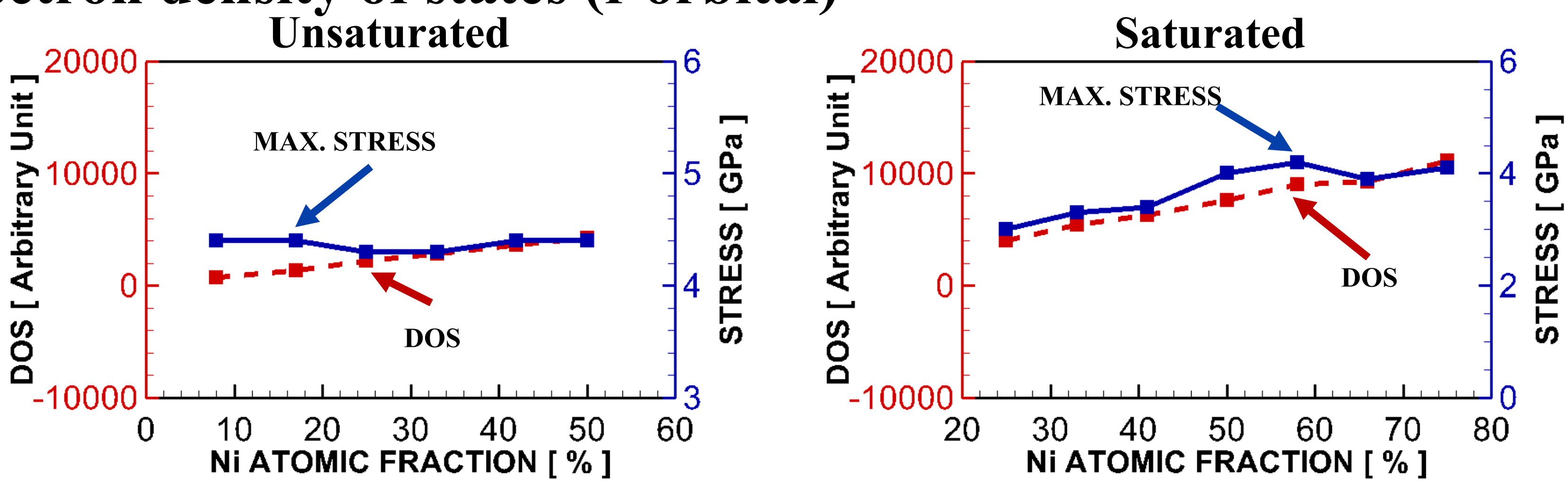

➢Phonon dispersion

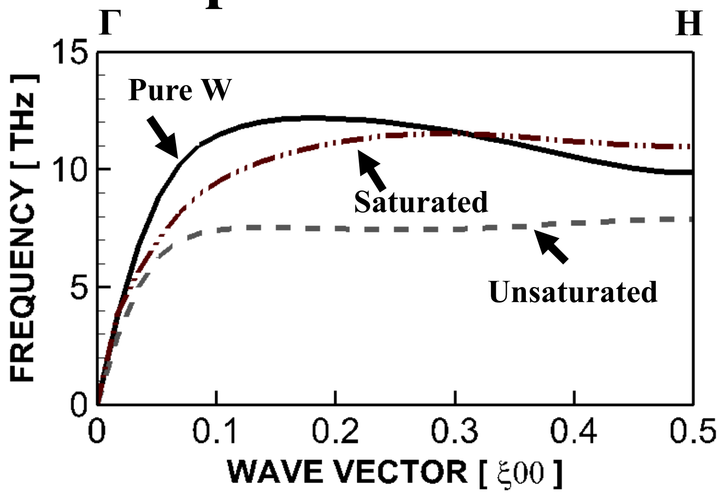

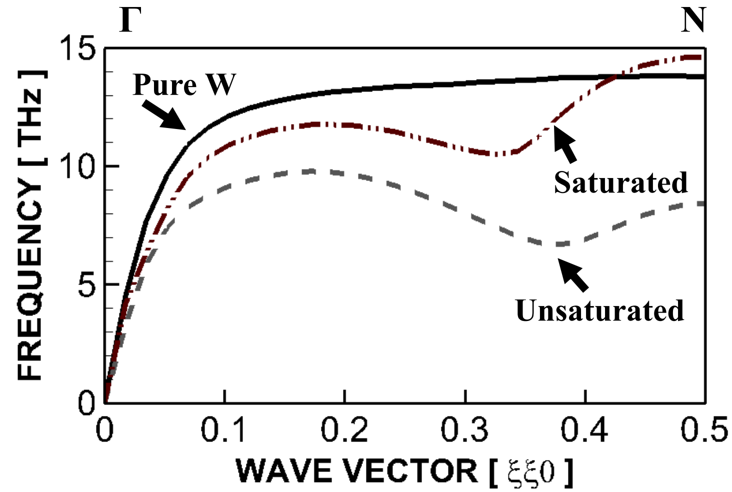

➢Prediction of peak tensile strength

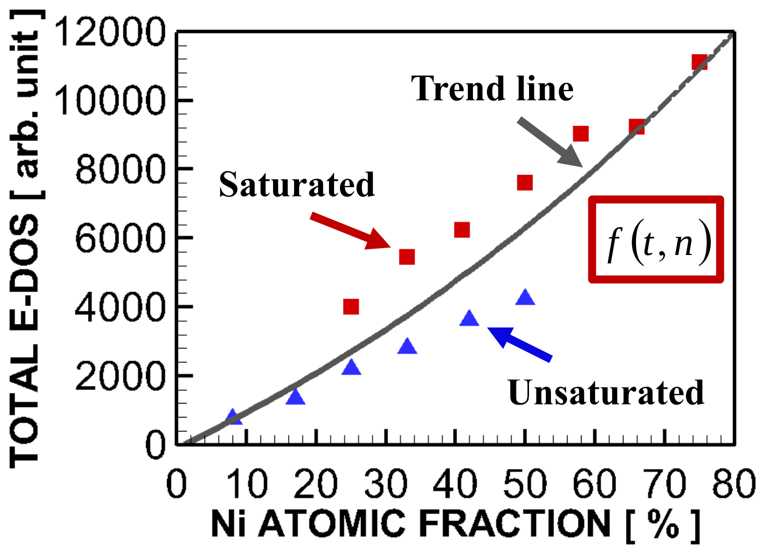

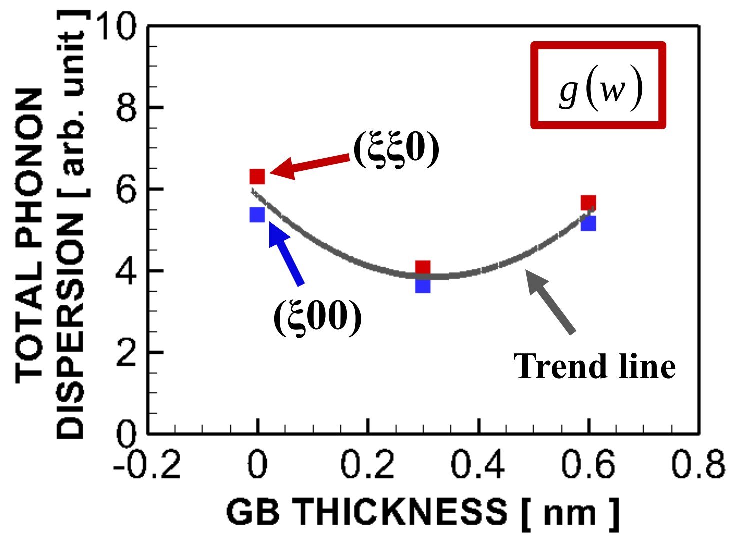

$$\frac{T_{max}}{T_{ideal}} = \cdot \frac{CE}{CD} \cdot \frac{1}{\Phi} \cdot f(t,n) \cdot g(w)$$

T_{max} : Maximum tensile strength of W-Ni alloy
T_{ideal} : Idealistic maximum tensile strength of W
Φ : Surface energy of W
CE : Atomic level cohesive energy of W

How does this prediction apply to continuum scale fracture?

➢Continuum scale model

(1) Nano-scale model

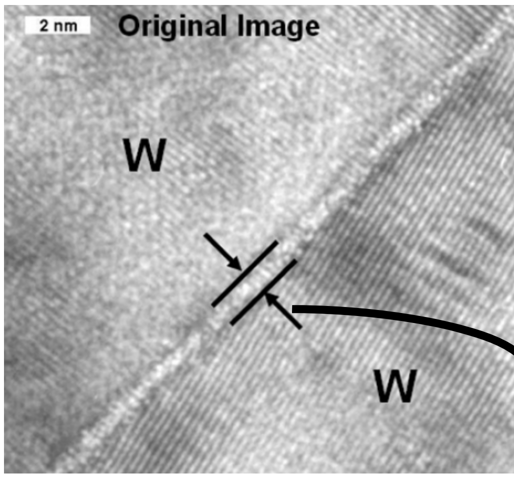

[V. Gupta et al, 2007]

Bi-granular model

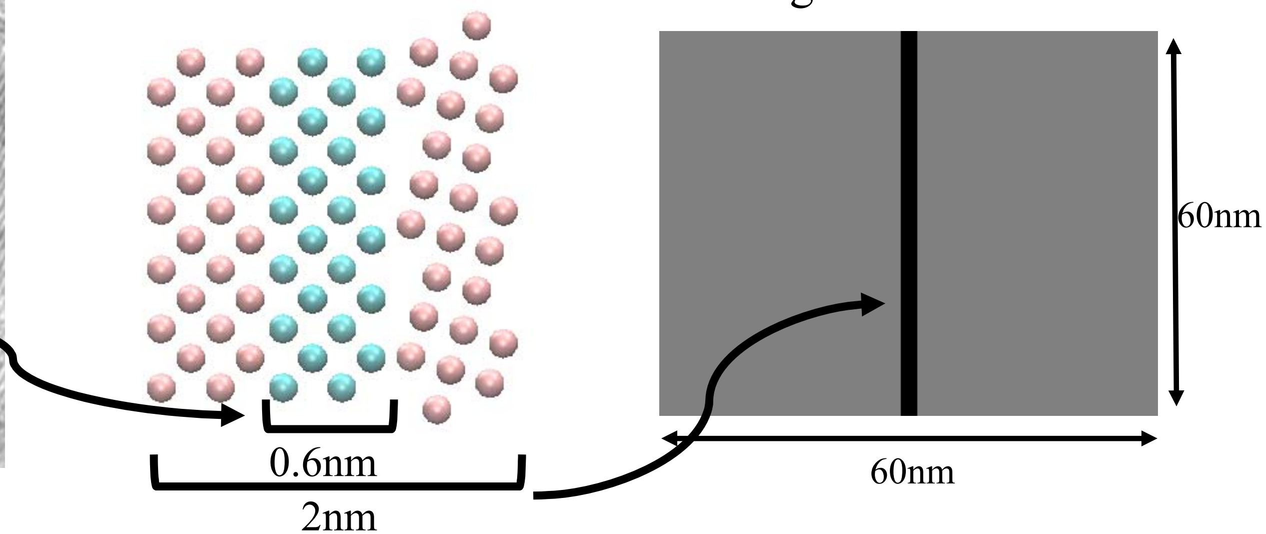

(2) Micro-scale model

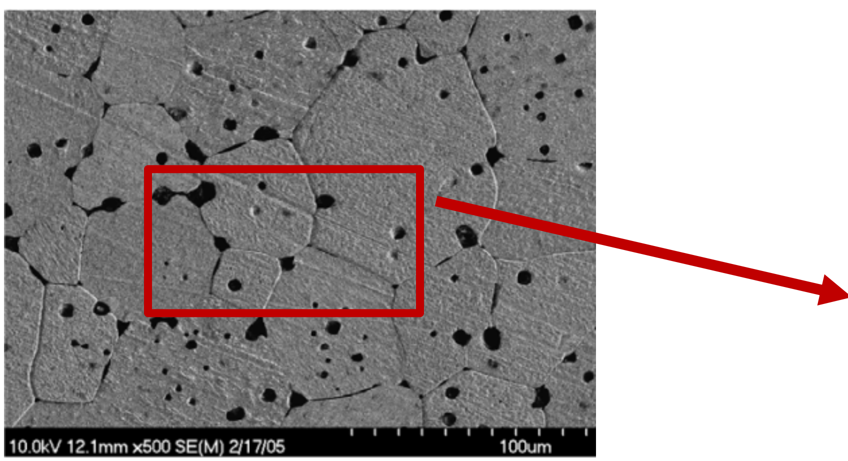

[V. Gupta et al, 2007]

Polycrystalline model

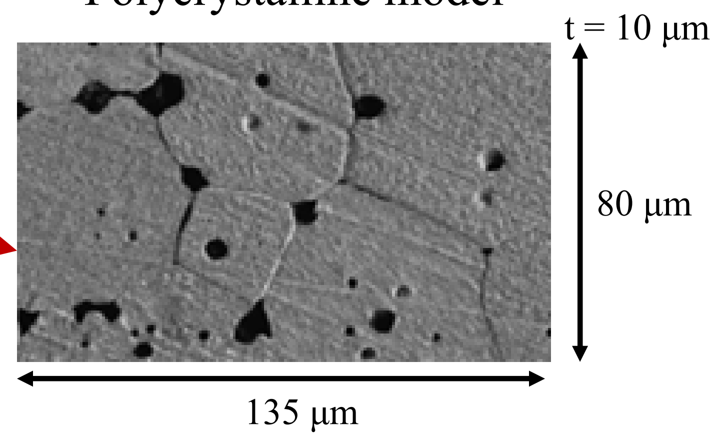

➢Material model of grains and GBs

Grain

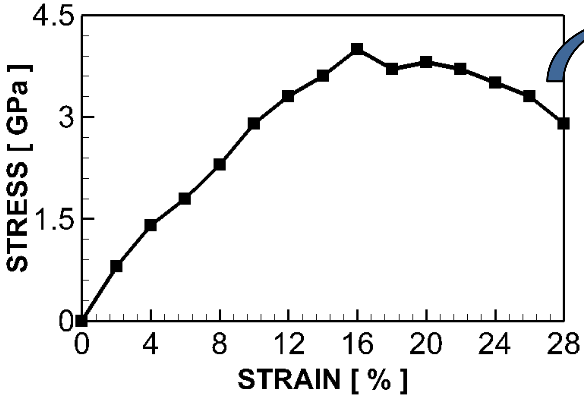

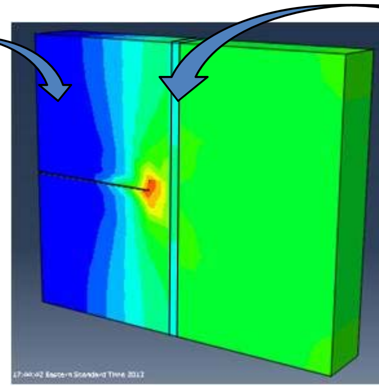

Grain boundary

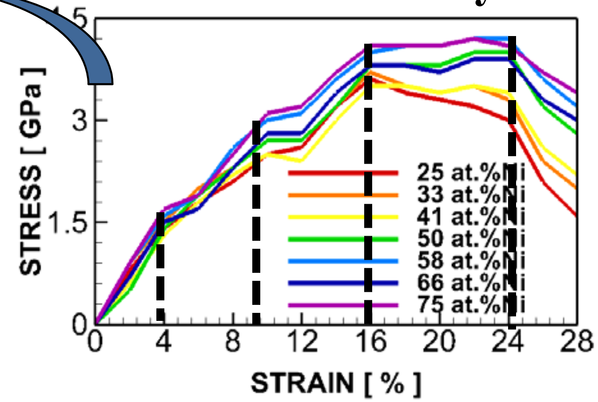

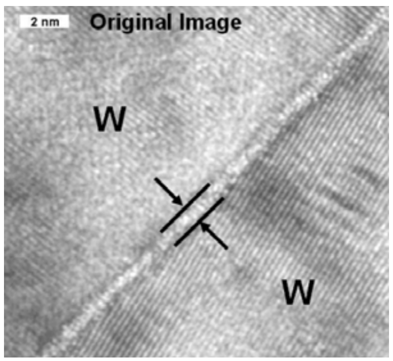

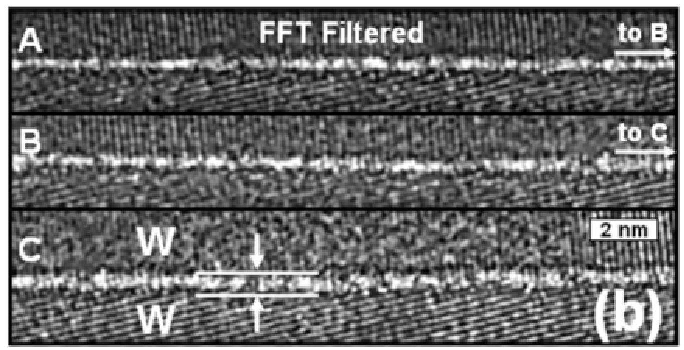

[V. Gupta et al, 2007]

Crack propagation of GB

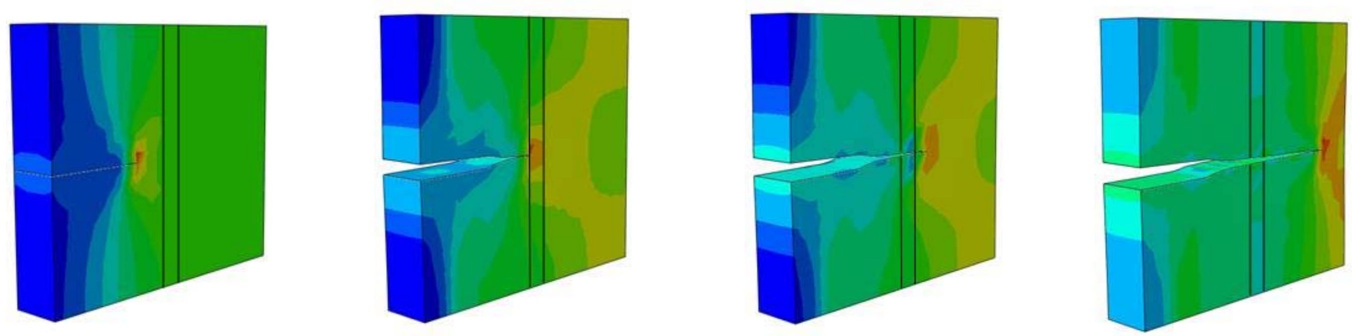

Time-step increment 4.5E-5 0.013 0.015 0.018

➢Fracture toughness analysis

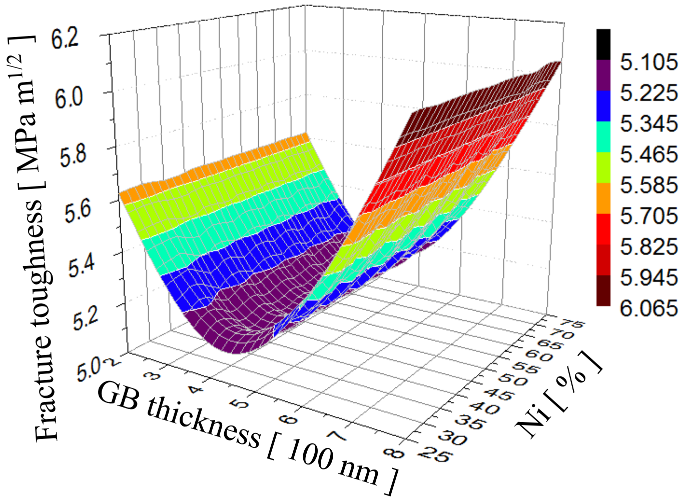

Fracture toughness in crack initiation

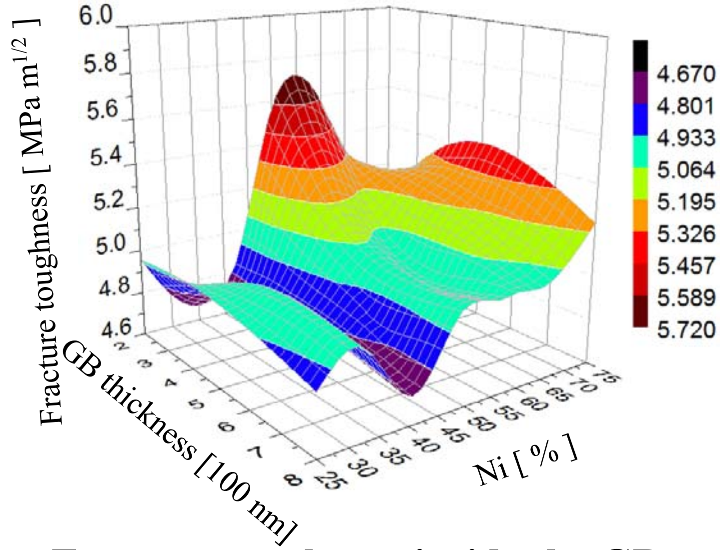

Fracture toughness inside the GB

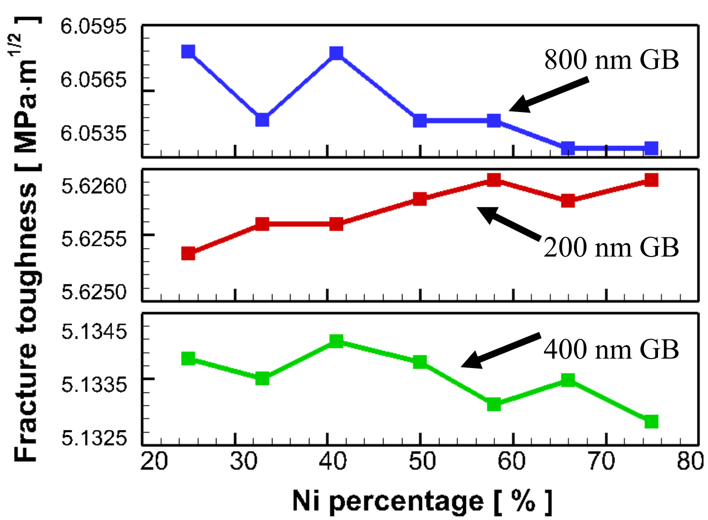

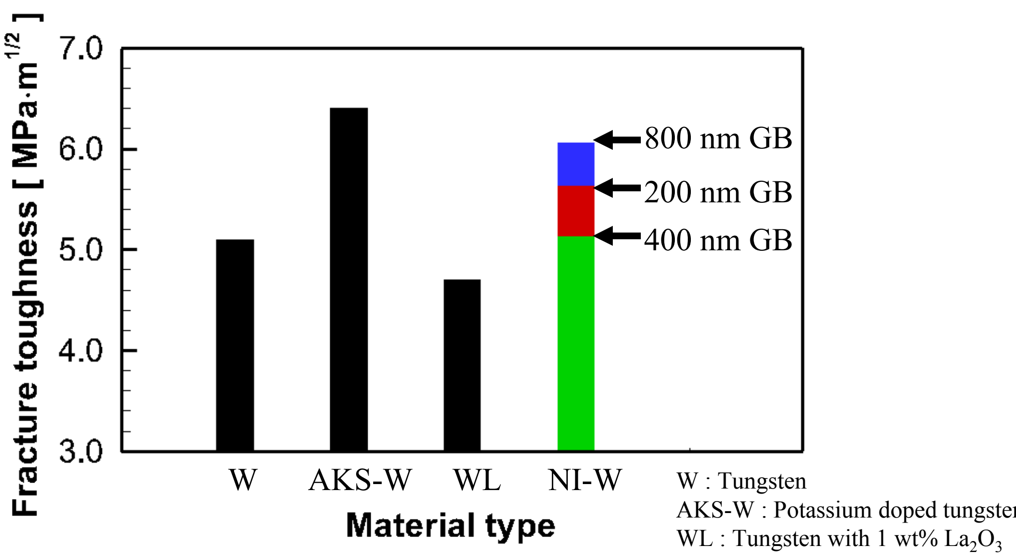

[B. Gludovatz and et al., 2010]

➢Brittleness index of GBs

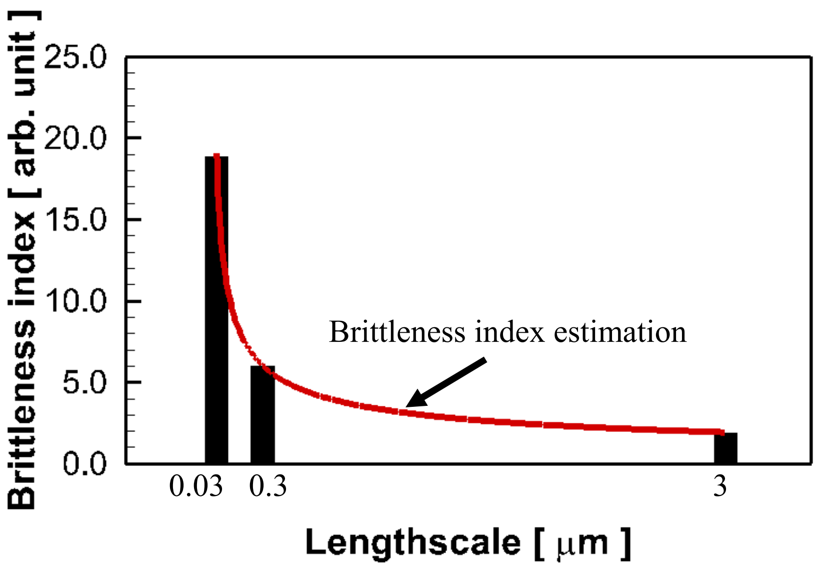

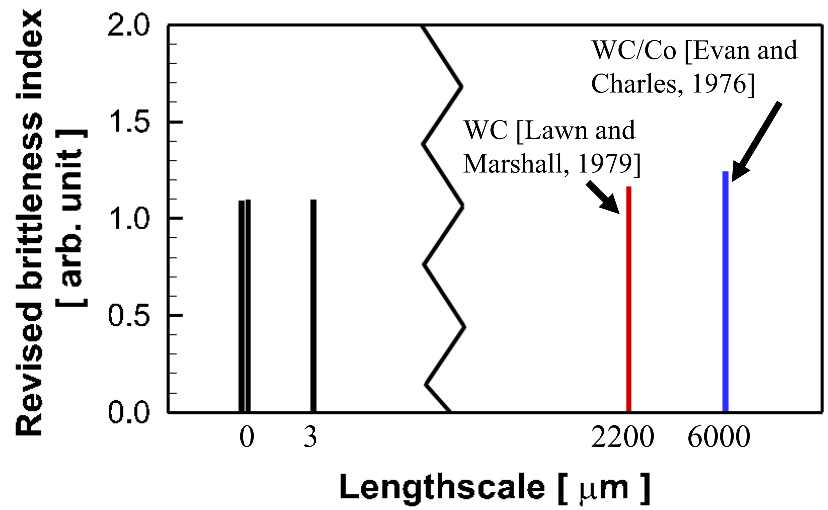

Effect of length-scale : $B = 3.3L^{-1/2}$

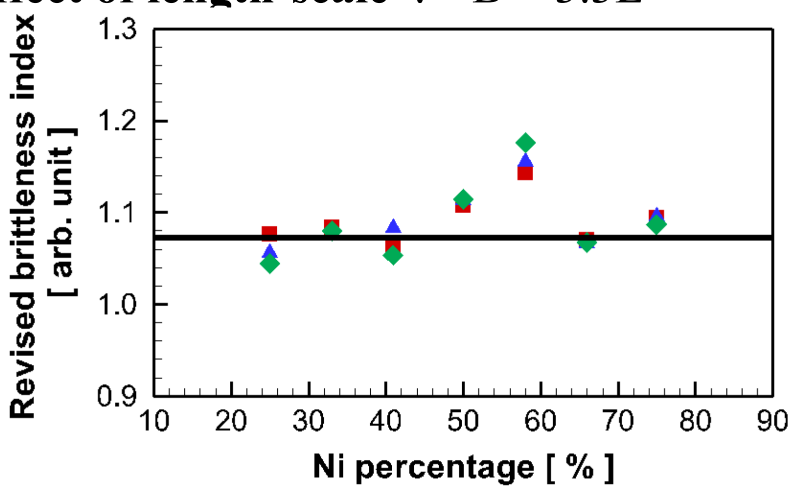

$$\boxed{B^* = \frac{H}{K_c} \cdot \frac{1}{\alpha} \sqrt{L}}$$

$\alpha = 3.3$ for W-Ni

Nomenclature

B*	brittleness index (no unit)
L	lengthscale (μm)
T	max. tensile strength (fracture strength)
H	hardness (GPa)
Kc	fracture toughness (MPa m^1/2)
t	GB thickness (μm)
p	Ni fraction (no unit)

- **Measurement of GB embrittlement has been obtained using the revised brittleness index.**
- **This provides an absolute range of qualitative measurement to describe the brittleness without considering the length scale limitations.**

➢Crack propagation in different angled GBs

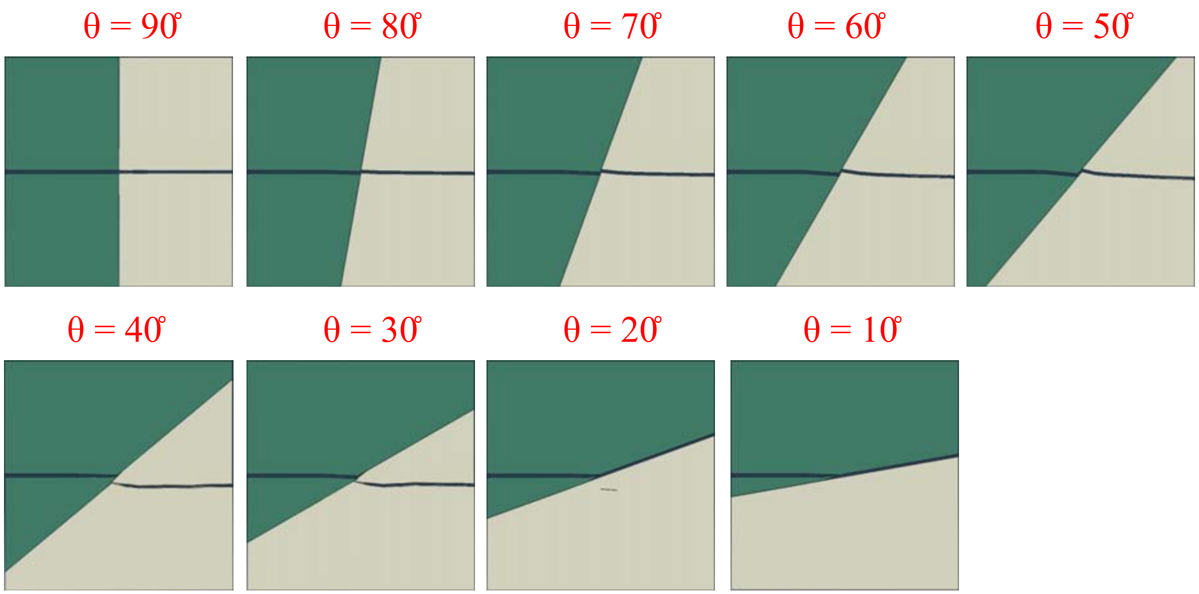

- ➢Inter-granular failure is represented as 1
- ➢Trans-granular failure is represented as -1

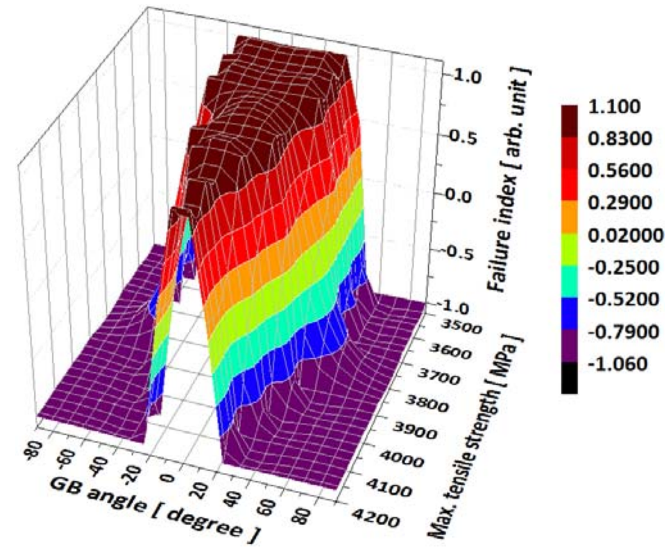

GB angle from -90 to 90 degree

❖**<u>Failure index</u>** : An index (between -1 and 1) to describe failure type, which can be either inter-granular failure or trans-granular failure.

$$FI = a + b\frac{T_{GB}}{T_{Grain}} + c\theta^2$$

a = 4.45
b = -4.2
c = -0.00024

Using the heavi-side function

$$H[FI] = \begin{cases} 1, & FI \geq 0 \\ -1, & FI < 0 \end{cases}$$

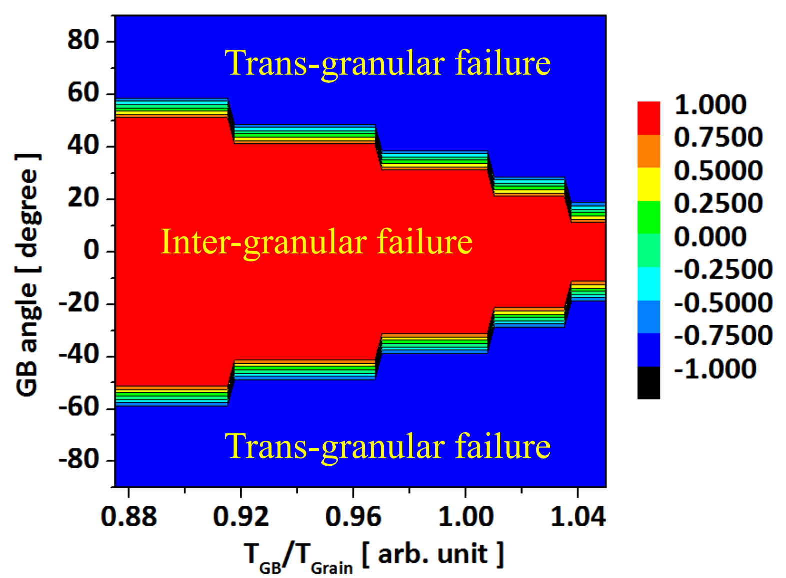

➢Validation and Conclusion

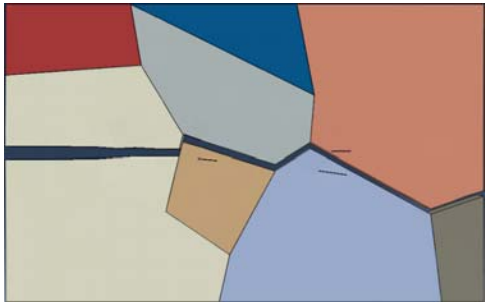

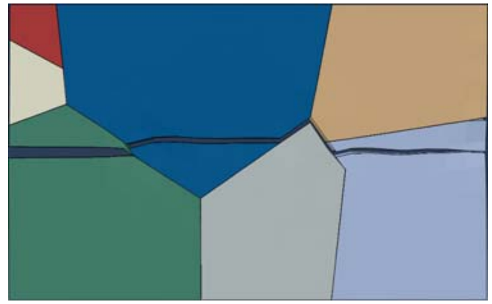

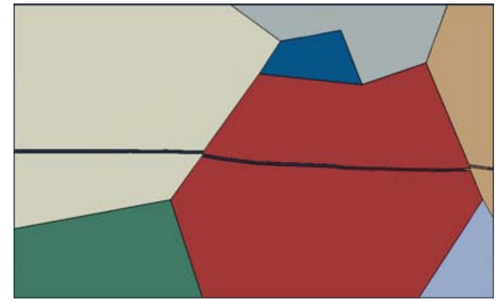

➢Perfect inter-granular failure has occurred.
➢Contains crack path with maximum GB angle of 67˚.
➢GB strength property can be predicted.

$$FI = a + b\frac{T_{GB}}{T_{Grain}} + c\theta^2$$

➢According to the failure index prediction, given microstructure has max. tensile strength ratio between GB and grain as $T_{GB} \leq (0.803)\cdot T_{Grain}$.

✓**For various failed morphologies of polycrystalline W-Ni, GB's strength property can be predicted using the derived failure type criteria.**

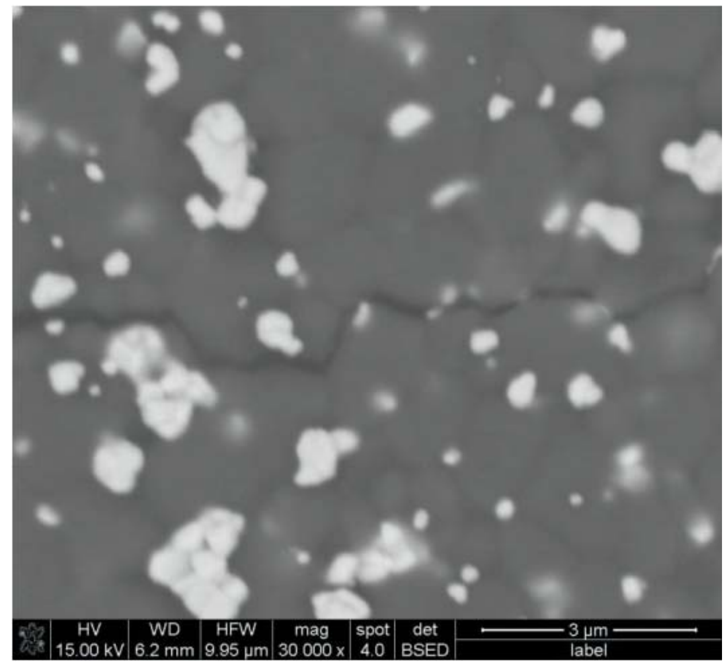

[Zbigniew Pedzich, 2012]

Evolution: Previous Works

- Microstructure evolution has been observed through experimental studies
  Groza, 2000; Hong, 2003; Dahl, 2007

- Simulation developed replicating the whole sintering process
  Maizza, 2007; Vanmeensel, 2005

- Kinetic Monte Carlo simulation applied to microstructural evolution: Probabilistic approach, depends on random sampling
  Olevsky, 2004

- Phase field modeling has been done to identify sintering mechanisms, external loading not considered
  Wang, 2006; Liu, 2011; Deng, 2012

- Consolidation kinetics has been captured experimentally
  Bruson, 1984; Grigoryev, 2009; Tang, 2013

Modeling Approach

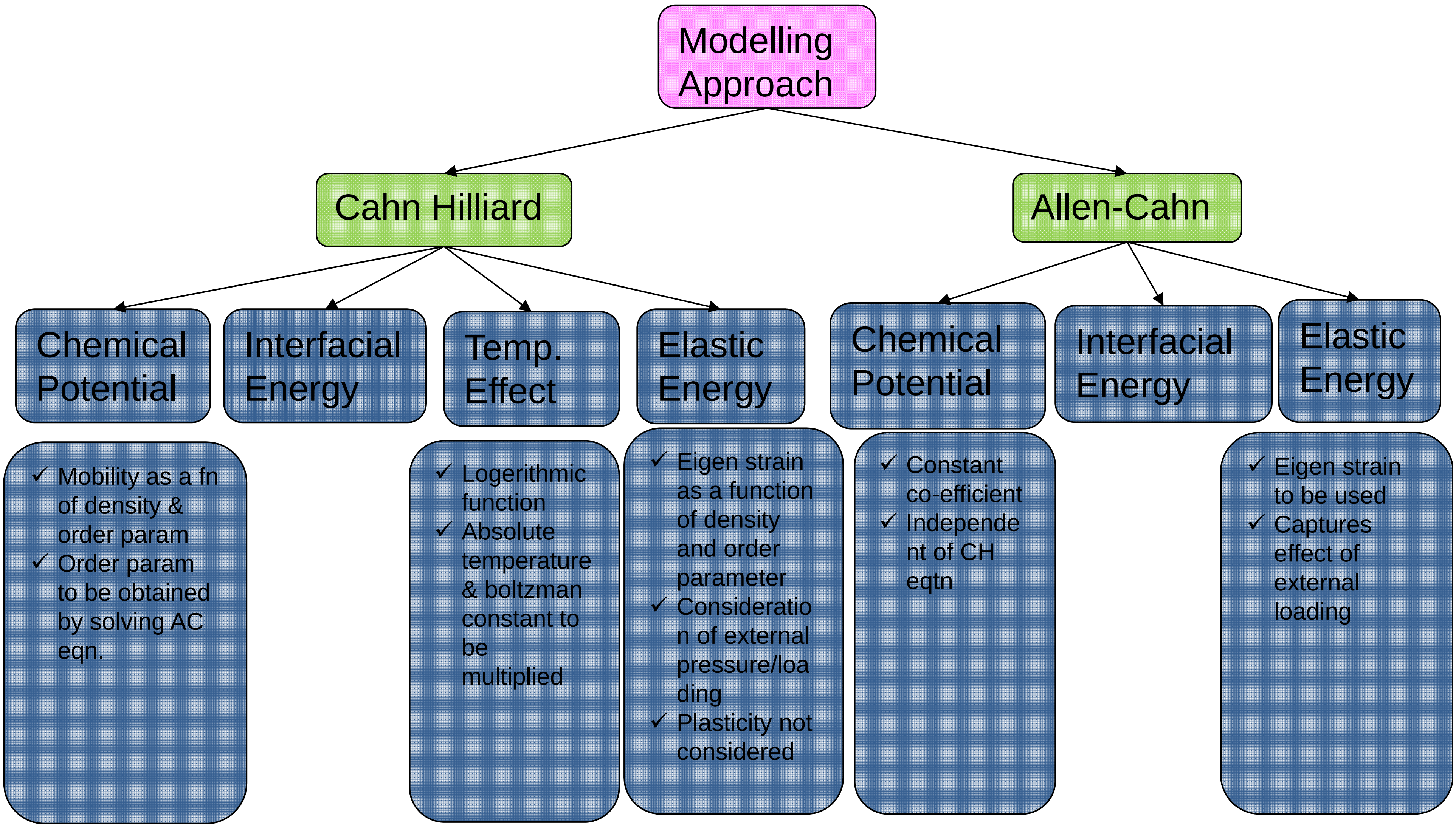

Moose Simulation

Mesh

- Rectangular grid will be created
- Corresponding Element types will assigned

Functions

- The phase field variables will be assigned
- Initial structure is created with assigned initial condition
- All the constants & their values can also be assigned in material section

Kernels

- Define the total free energy expressions, use in-built Allen-Cahn & Cahn-Hilliard equations
- Calculate derivatives & give them as input

Executioner

- Define solver type: Finite Difference Method
- Assign pre-conditioning if required

Post-process

- Micro-structural images
- Plot for temporal evolution of phase field variable
- Calculate evolution of grain size

Simulation Details: Test Run

- ✓ Simulation block: 100X60; Particle Radius: 20 & 20;
- ✓ Grid Size: 0.5
- ✓ Total Time: 60 with Time Step: 1.0
- ✓ Maximum displacement applied 35 µm

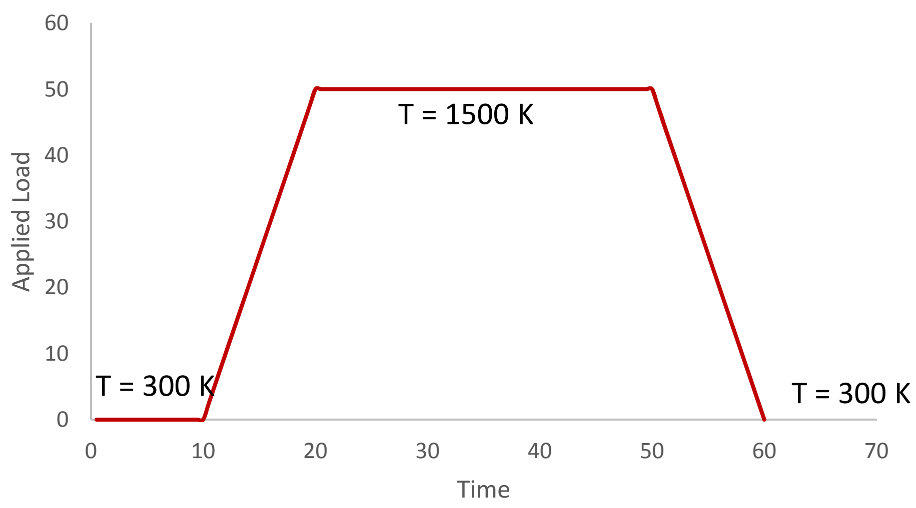

Test Results: DensityVariation w/o load

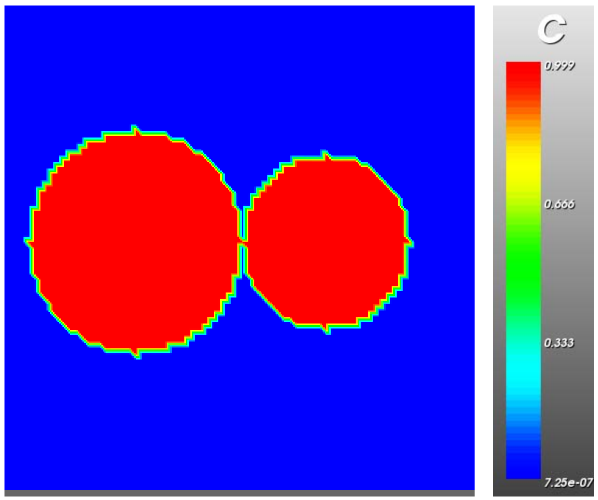

Initial Condition

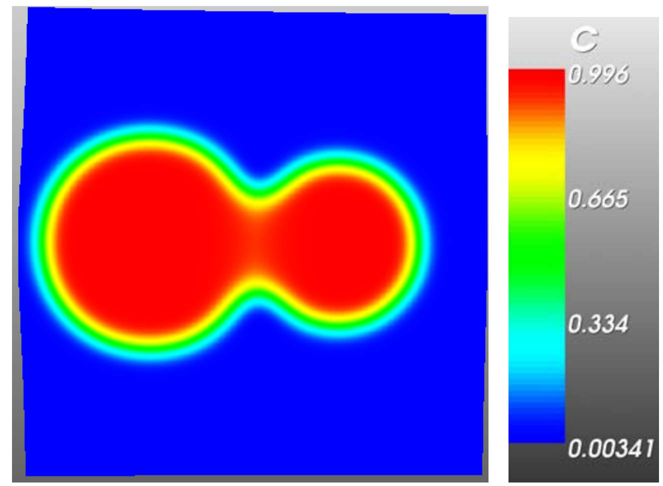

Time = 0.5

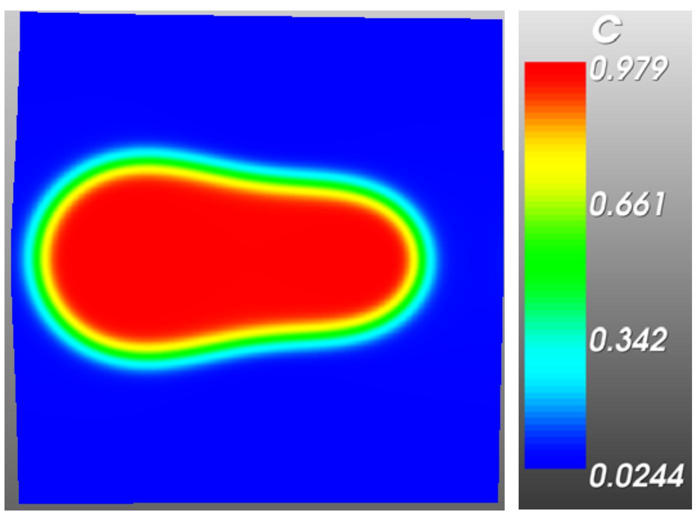

Time = 20.5

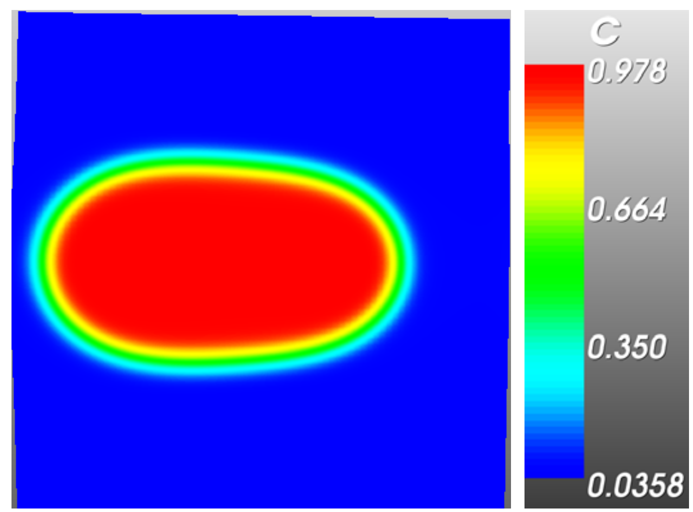

Time = 60.0

Test Results: DensityVariation w/ load

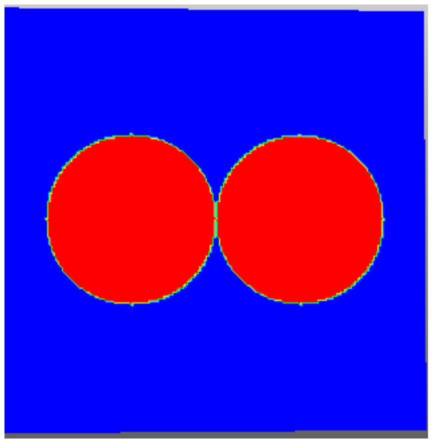

Initial Condition

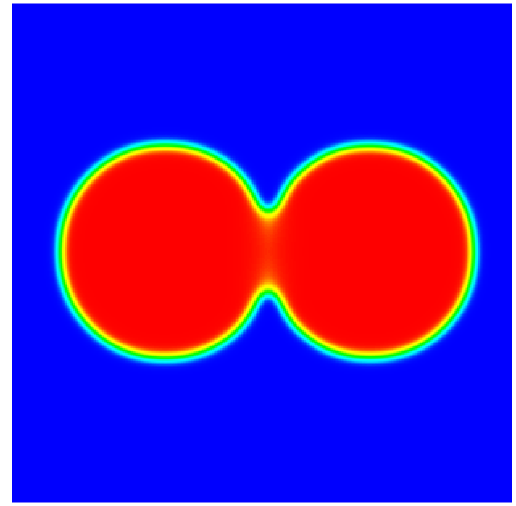

Time = 1.0

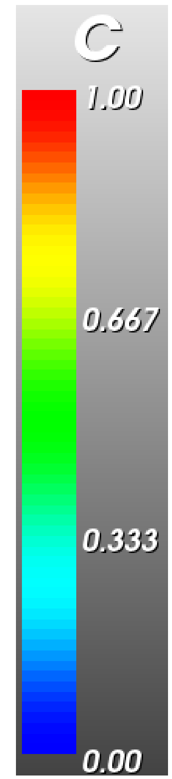

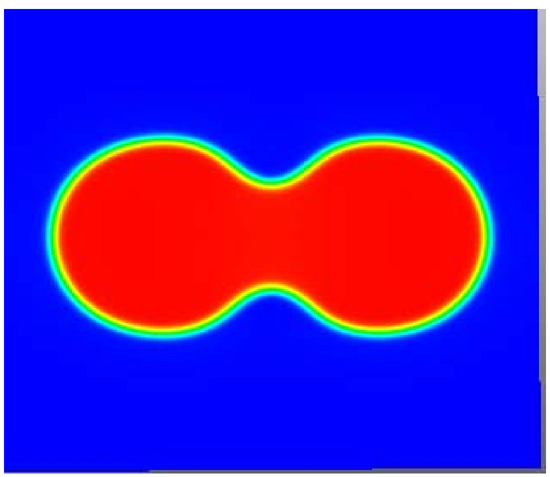

Time = 14

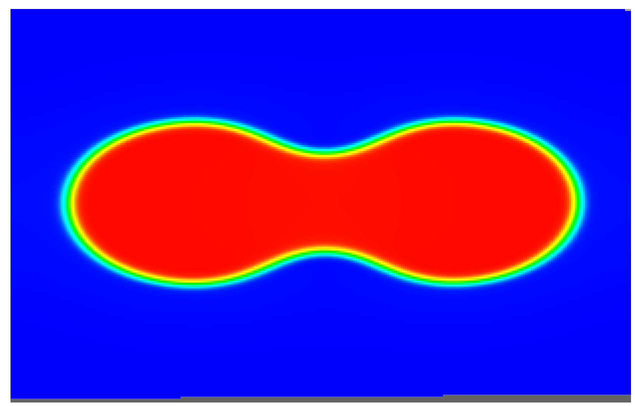

Time = 35.0

Summary

- All Tasks on Schedule
- A Grain Boundary Diagram Based Approach for long term GB evolution identified
- A Brittleness Index parameter identified to predict effect of GB on microstructural Strength
- Control sample manufacturing process established
- In-situ and ex-situ experimentation protocols established
- 4 international journal publications, 1 PhD graduate, 3 supported students with grant in second year